Mon. Not. R. Astron. Soc. **316**, 749–767 (2000)

The European Large Area *ISO* Survey – I. Goals, definition and observations

Seb Oliver,[1★†] Michael Rowan-Robinson,[1] D. M. Alexander,[2] O. Almaini,[3] M. Balcells,[4] A. C. Baker,[5] X. Barcons,[6] M. Barden,[7] I. Bellas-Velidis,[8] F. Cabrera-Guerra,[4] R. Carballo,[6,9] C. J. Cesarsky,[10] P. Ciliegi,[11] D. L. Clements,[5] H. Crockett,[1] L. Danese,[2] A. Dapergolas,[8] B. Drolias,[1] N. Eaton,[1] A. Efstathiou,[1] E. Egami,[12] D. Elbaz,[10] D. Fadda,[10] M. Fox,[1] A. Franceschini,[13] R. Genzel,[7] P. Goldschmidt,[1] M. Graham,[1] J. I. Gonzalez-Serrano,[6] E. A. Gonzalez-Solares,[4] G. L. Granato,[13] C. Gruppioni,[11] U. Herbstmeier,[14] P. Héraudeau,[14] M. Joshi,[1] E. Kontizas,[8] M. Kontizas,[15] J. K. Kotilainen,[16] D. Kunze,[7] F. La Franca,[17] C. Lari,[18] A. Lawrence,[3] D. Lemke,[14] M. J. D. Linden-Vørnle,[19,20] R. G. Mann,[1] I. Márquez,[21] J. Masegosa,[21] K. Mattila,[22] R. G. McMahon,[23] G. Miley,[24] V. Missoulis,[1] B. Mobasher,[1] T. Morel,[1] H. Nørgaard-Nielsen,[20] A. Omont,[25] P. Papadopoulos,[24] I. Perez-Fournon,[4] J-L. Puget,[26] D. Rigopoulou,[7] B. Rocca-Volmerange,[25] S. Serjeant,[1] L. Silva,[2] T. Sumner,[1] C. Surace,[1] P. Vaisanen,[22] P. P. van der Werf,[24] A. Verma,[1] L. Vigroux,[10] M. Villar-Martin[25] and C. J. Willott[4]

[1]*Astrophysics Group, Blackett Laboratory, Imperial College of Science Technology & Medicine (ICSTM), Prince Consort Rd, London SW7 2BZ*
[2]*SISSA, International School for Advanced Studies, Via Beirut 2-4, 34014 Trieste, Italy*
[3]*Institute for Astronomy, University of Edinburgh, Royal Observatory, Blackford Hill, Edinburgh EH9 3HJ*
[4]*Instituto de Astrofisica de Canarias, C/ Via Lactea, s/n, 38200 La Laguna, S/C de Tenerife, Spain*
[5]*Dept of Physics & Astronomy, Cardiff University, PO Box 913, Cardiff CF24 3YB*
[6]*Instituto de Fúsica de Cantabria (Consejo Superior de Investigaciones Cientúficas – Universidad de Cantabria), 39005 Santander, Spain*
[7]*Max-Planck-Institut für extraterrestrische Physik, Postfach 1603, 85740 Garching, Germany*
[8]*National Observatory of Athens, Astronomical Institute, PO Box 20048, GR-11810, Greece*
[9]*Departamento de Fúsica Moderna, Universidad de Cantabria, 39005 Santander, Spain*
[10]*CEA/SACLAY, 91191 Gif sur Yvette cedex, France*
[11]*Osservatorio Astronomico di Bologna, via Ranzani 1, 40127 Bologna, Italy*
[12]*Infrared Astronomy Group, 320-47 Downs Laboratory of Physics, California Institute of Technology, Pasadena, CA 91125, USA*
[13]*Dipartimento di Astronomia, Universita' di Padova, Vicolo Osservatorio 5, I-35122 Padova, Italy*
[14]*Max-Planck-Institut für Astronomie, Königstuhl (MPIA) 17, D-69117 Heidelburg, Germany*
[15]*Section of Astrophysics, Astronomy & Mechanics, Dept. of Physics, University of Athens, Panepistimiopolis, GR-15783, Zografos, Greece*
[16]*Tuorla Observatory, University of Turku, Väisäläntie 20, FIN-21500 Piikkiö, Finland*
[17]*Dipartimento di Fisica, Universita degli Studi 'Roma TRE' Via della Vasca Navale 84, I-00146 Roma, Italy*
[18]*Institute di Radio Astronomy, Bologna, Italy*
[19]*Niels Bohr Institute for Astronomy, Physics and Geophysics, Astronomical Observatory, Juliane Maries Vej 30, DK–2100 Copenhagen Ø, Denmark*
[20]*Danish Space Research Institute, Juliane Maries Vej 30, DK–2100 Copenhagen Ø, Denmark*
[21]*Instituto de Astrofísica de Andalucía, CSIC, Apartado 3004, E-18080 Granada, Spain*
[22]*Observatory, PO Box 14, Tahtitorninmaki, FIN-00014 University of Helsinki, Finland*
[23]*Institute of Astronomy, The Observatories, Madingley Road, Cambridge CB3 0HA*
[24]*Leiden Observatory, PO Box 9513, NL-2300 RA Leiden, the Netherlands*
[25]*Institut d'Astrophysique de Paris, 98bis Boulevard Arago, F 75014 Paris, France*
[26]*Institut d'Astrophysique Spatiale (IAS), Bâtiment 121, Université Paris XI, 91405 Orsay cedex, France*

Accepted 2000 March 15. Received 1999 October 20; in original form 1999 July 22

★ E-mail: S.Oliver@Sussex.ac.uk
† Current address: Astronomy Centre, Physics and Astronomy Subject Group, School of CPES, University of Sussex, Falmer, Brighton BN1 9QJ.

ABSTRACT

We describe the European Large Area *ISO* Survey (ELAIS). ELAIS was the largest single Open Time project conducted by *ISO*, mapping an area of 12 $\deg^2$ at 15 μm with ISOCAM and at 90 μm with ISOPHOT. Secondary surveys in other *ISO* bands were undertaken by the ELAIS team within the fields of the primary survey, with 6 $\deg^2$ being covered at 6.7 μm and 1 $\deg^2$ at 175 μm.

This paper discusses the goals of the project and the techniques employed in its construction, as well as presenting details of the observations carried out, the data from which are now in the public domain. We outline the ELAIS 'preliminary analysis' which led to the detection of over 1000 sources from the 15 and 90-μm surveys (the majority selected at 15 μm with a flux limit of $\sim$3 mJy), to be fed into a ground-based follow-up campaign, as well as a programme of photometric observations of detected sources using both ISOCAM and ISOPHOT.

We detail how the ELAIS survey complements other *ISO* surveys in terms of depth and areal coverage, and show that the extensive multi-wavelength coverage of the ELAIS fields resulting from our concerted and on-going follow-up programme has made these regions amongst the best studied areas of their size in the entire sky, and, therefore, natural targets for future surveys. This paper accompanies the release of extremely reliable subsets of the 'preliminary analysis' products. Subsequent papers in this series will give further details of our data reduction techniques, reliability and completeness estimates and present the 15- and 90-μm number counts from the 'preliminary analysis', while a further series of papers will discuss in detail the results from the ELAIS 'final analysis', as well as from the follow-up programme.

Key words: surveys – galaxies: active – galaxies: evolution – galaxies: starburst – infrared: galaxies – infrared: stars.

1 INTRODUCTION

The *Infrared Space Observatory* (*ISO*, Kessler et al. 1996) was the natural successor to the *Infrared Astronomical Satellite* (*IRAS*), and has primarily been used to undertake detailed studies of individual objects and regions. However, *ISO* also provided an opportunity to perform survey work at sensitivities beyond the reach of *IRAS*. The *IRAS* survey was of profound significance for cosmology, extragalactic astrophysics and for the study of stars, star-forming regions and the interstellar medium in the Galaxy. The mapping of large-scale structure (Saunders et al. 1991) in the galaxy distribution, the discovery of ultra-luminous infrared galaxies (see the review by Sanders & Mirabel 1996) and of hyper-luminous infrared galaxies like *IRAS* F10214+4724 (Rowan-Robinson et al. 1991a), and the detection of proto-planetary discs around fairly evolved stars, were all unexpected discoveries of the *IRAS* survey. The $z = 2.3$ galaxy F10214+4724, was at the limit of detectability by *IRAS* ($S_{60} \gtrsim 0.2$ Jy). Several other $z > 1$ galaxies and quasars have now been found from follow-up of faint *IRAS* samples. Recent submillimetre surveys, in particular with SCUBA on the JCMT (e.g. Smail, Ivison & Blain 1997; Barger et al. 1998; Hughes et al. 1998; Blain et al. 1999; Eales et al. 1999), are detecting sources which are probably very high redshift counterparts to these *IRAS* sources. Pointed observations of high redshift quasars and radio galaxies produce detections at submillimetre wavelengths in continuum and line emission, but mostly lie below the limit of the *IRAS* survey at far-infrared wavelengths.

While designed as an observatory instrument, the huge improvement in sensitivity provided by *ISO* offered the opportunity to probe the galaxy population to higher redshift than *IRAS* and to make progress in understanding the obscured star formation history of the Universe. A significant fraction of the mission time was thus spent on field surveys. In this paper we describe the 'European Large Area *ISO* Survey' (ELAIS) which represents the largest non-serendipitous survey conducted with *ISO*. This survey provides a link between the *IRAS* survey, the deeper *ISO* surveys and the submillimetre surveys.

ELAIS is a collaboration involving 25 European institutes, led from Imperial College. This project surveyed around 12 $\deg^2$ of the sky at 15 and 90 μm nearly 6 $\deg^2$ at 6.7 μm together with a further 1 $\deg^2$ at 175 μm. The survey used the *ISO* Camera (ISOCAM, Cesarsky et al. 1996) at the two shorter wavelengths and the *ISO* Photometer (ISOPHOT, Lemke et al. 1996) at the longer wavelengths. ELAIS was the largest open time project undertaken by *ISO*: a total of 375 h of scientifically validated data have been produced. We have detected over 1000 extragalactic objects and a similar number of Galactic sources. Around 200 of these objects have been re-observed with *ISO* to provide detailed mid/far-infrared photometry.

This paper outlines the broad scientific objectives of this project and describes the selection of the observing modes and survey fields. It also details the execution of the *ISO* observations and briefly outlines the data reduction and data products. Finally we show how this survey complements other *ISO* surveys and summarize the extensive multi-wavelength programmes taking place in the ELAIS fields.

2 KEY SCIENTIFIC GOALS

2.1 The star formation history of the Universe

The main extragalactic population detected by *IRAS* was galaxies with high rates of star formation. These objects are now known to evolve with a strength comparable to active galactic nuclei (AGN) (e.g. Oliver et al. 1995). The distance to which these objects were visible to *IRAS* was, however, insufficient to determine the nature of their evolution. The sensitivity of *ISO* allows us to detect these objects at much higher redshifts and thus obtain greater understanding of the cosmological history of star formation. The infrared luminosity provides a better estimate of the total star formation rate than optical and UV estimators (e.g. Madau et al. 1996) as these monitor star formation only from regions with low obscuration and require large corrections for extinction (Steidel et al. 1999). Another important star formation indicator for galaxies is radio luminosity (e.g. Condon 1992). For galaxies obeying the well known far-infrared radio correlation (Helou, Soifer & Rowan-Robinson 1985), the depth of the survey described here is well matched to that of sub-mJy radio surveys (e.g. Condon & Mitchell 1984; Windhorst 1984; Windhorst et al. 1985; Hopkins et al. 1998; Gruppioni, Mignoli & Zamorani 1999a). Comparison of the global star formation rate determined in the infrared with other determinations from the optical and UV luminosity densities, Hα luminosity density, radio luminosity density, etc. will give a direct estimate of the importance of dust obscuration, vitally important for models of cosmic evolution, as well as providing us with a reliable estimate for the total star formation rate. The ELAIS follow-up surveys (see Section 7) will allow us to go a stage further and apply a number of these complementary star formation tracers to the same volume and in many cases on the same objects, thereby addressing the impact of dust extinction independently of any peculiarities to any particular survey volume.

Figs 1–3 show the predicted redshift distribution of star-forming galaxies in the ELAIS survey selected at 15, 90 and 175 μm. The predictions come from three different evolutionary models; the first model is that of Pearson & Rowan-Robinson (1996), the second and third are models 'A' and 'E' from Guiderdoni et al. (1998). All three models are extrapolations from *IRAS* data. The total number of objects of various different types predicted by two of these models and a third from Franceschini et al. (1994), are also tabulated in Table 1. While the source counts from ELAIS alone may not be able to distinguish between such models, spectroscopic identifications, source classifications and the redshift distributions will.

2.2 Ultra-luminous infrared galaxies at high z

IRAS uncovered a population with enormous far-infrared luminosities, $L_{\rm FIR} > 10^{12}\,{\rm L}_{\odot}$ (see the review by Sanders & Mirabel 1996). While somewhere between 20 and 50 per cent of these objects appear to have an AGN (Veilleux et al. 1995; Lawrence et al. 2000; Sanders, Surace & Ishida 1999; Veilleux, Kim & Sanders 1999) it is still a source of controversy as to whether the illumination of the dust arises principally from an AGN or a starburst. *ISO* spectra of samples of ultra-luminous infrared galaxies (Genzel et al. 1998; Lutz et al. 1998; Lutz, Veilleux & Genzel 1999; Rigopoulou et al. 1999) appear to demonstrate that while some do require the photoionization energies typical for AGN to explain the obscured lines, most are consistent with

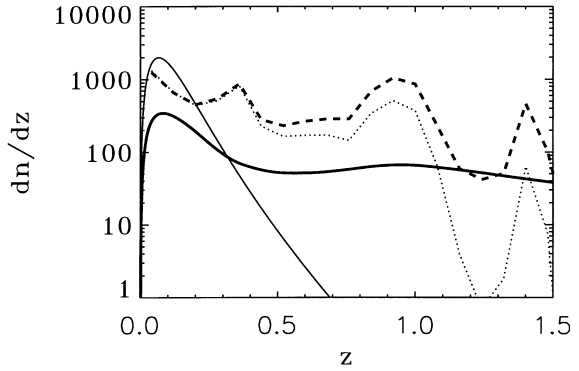

Figure 1. Expected populations and redshift distribution for the 15-μm survey assuming a depth of 3 mJy over 11 deg^2. The redshift distribution is plotted as dn/dz in dimensionless units. Cirrus (solid line) and starburst (thick solid line) components are from a model similar to Oliver, Rowan-Robinson & Saunders (1992) and Pearson & Rowan-Robinson (1996), model *E* (dashed line) and model *A* (dotted line) are from Guiderdoni et al. (1998).

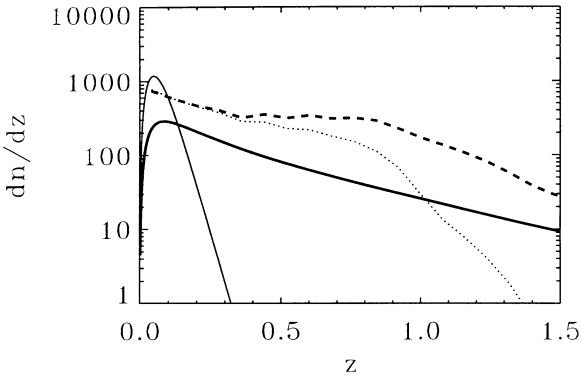

Figure 2. Expected populations and redshift distribution for the 90-μm survey, assuming a depth of 100 mJy over 11 deg^2. The redshift distribution is plotted as dn/dz in dimensionless units. Cirrus (solid line) and starburst (thick solid line) components are from a model similar to Oliver et al. (1992) and Pearson & Rowan-Robinson (1996), model *E* (dashed line) and model *A* (dotted line) are from Guiderdoni et al. (1998).

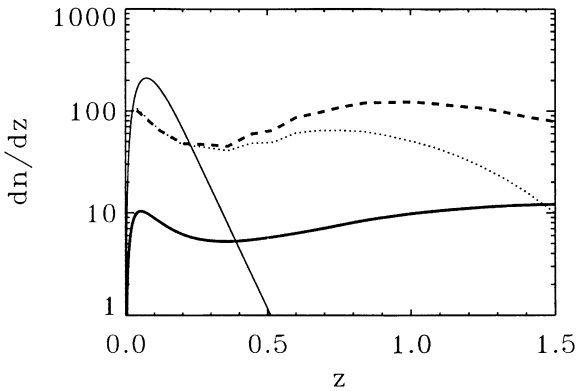

Figure 3. Expected populations and redshift distribution for the 175-μm survey, assuming a depth of 75 mJy over 1 deg^2. The redshift distribution is plotted as dn/dz in dimensionless units. Cirrus (solid line) and starburst (thick solid line) components are from a model similar to Oliver et al. (1992) and Pearson & Rowan-Robinson (1996), model *E* (dashed line) and model *A* (dotted line) are from Guiderdoni et al. (1998).

Table 1. Expected numbers of extragalactic sources from three a priori evolutionary models. Survey areas of 6, 11, 11 and 3 and depths of 1, 3, 100, 75 mJy in the 6.7, 15, 90 and 175-μm bands, respectively (roughly those achieved in our preliminary analysis) are asumed. The Pearson & Rowan-Robinson (1996) models do not include elliptical populations, the predictions at 175 μm are in fact calculated at 200 μm. The Franceschini et al. (1994) models were not available for longer wavelengths; the Guiderdoni et al. model (1998) is their strongly evolving model 'E', while their models include objects of different luminosities and SEDs their results do not discriminate so we arbitrarily assign them all to the star-forming row.

Model	Pearson & Rowan-Robinson (1996)	Franceschini et al. (1994)	Guiderdoni et al. (1998)
		6.7 μm	
Elliptical		8	
Normal spiral	455	38	
Star-forming galaxies	122		
AGN	64	31	
		15 μm	
Elliptical		11	
Normal spiral	308	378	
Star-forming galaxies	181	177	258
AGN	112	14	
		90 μm	
Elliptical			
Normal spiral	106		
Star-forming galaxies	109		231
AGN			
		175μm	
Elliptical			
Normal spiral	102		
Star-forming galaxies	76		261
AGN			

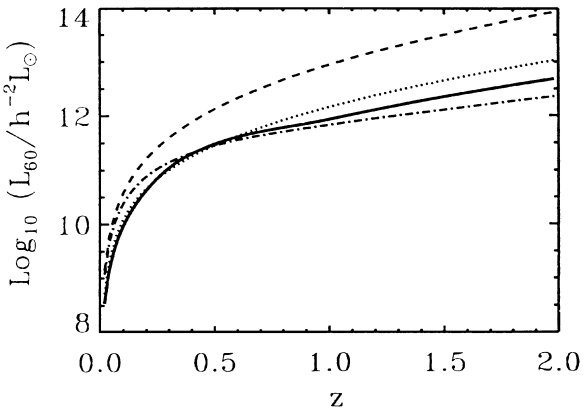

Figure 4. The minimum rest-frame 60-μm luminosity for a source with a starburst spectrum detectable in the ELAIS survey at $S_{15} > 3$ mJy (solid line), $S_{90} > 100$ mJy (dotted line), $S_{175} > 75$ mJy (dot-dashed line) and in the *IRAS* survey $S_{60} > 250$ mJy (dashed line).

starburst models. Interestingly, most of these objects appear to be in interacting systems, suggesting a mechanism that could trigger either an AGN, a starburst, or indeed both (e.g. Sanders et al. 1988; Lawrence et al. 1989; Leech et al. 1994; Clements et al. 1996).

The area of this survey is small compared to that of *IRAS* so we would not expect to detect large numbers of these objects. The Pearson & Rowan-Robinson (1996) model would predict that we would detect between 40 and 80 of these objects, although models such as that of Guiderdoni et al. (1998), which takes into account the increase in temperature of the dust with increasing luminosity, would predict more. Nevertheless such objects will be visible at greater distances than they were in *IRAS* and even a few examples at higher redshift would be interesting. Assuming a starburst SED (Rowan-Robinson & Efstathiou 1993) an object of $L_{60} = 10^{12}\,L_{\odot}$ ($H_0 = 50, q_0 = 1/2$) would be visible ($S_{15} > 3$ mJy) in the ELAIS survey to $z = 0.5$, where it is only visible to $z = 0.26$ in the *IRAS* Faint Source Catalogue ($S_{60} > 0.2$ Jy) and to $z = 0.15$ in the *IRAS* Point Source Catalogue ($S_{60} > 0.6$ Jy). ELAIS thus allows us to study samples of these controversial objects at higher redshift where both AGN and star formation are known to be enhanced. Fig. 4 shows the minimum 60-μm luminosity of a source which could be detected in both the ELAIS survey and the *IRAS* survey as a function of redshift.

2.3 Emission from dusty tori around AGN

The orientation-based unified models of AGN involve a central engine surrounded by an optically and geometrically thick torus (Antonucci & Miller 1985; Scheuer 1987; Barthel 1989; Antonucci 1993). In this model the optical properties of the central regions are dependent on the inclination angle of the torus, with type-2 objects defined as those with the central nucleus obscured by the torus, and type-1 objects (such as quasars) as those with an unobscured view of the nucleus. Objects with radio jets have the jets aligned approximately with the torus symmetry axis. The scheme is very attractive in providing a single conceptual framework for what would otherwise appear to be extremely diverse populations, and the models have survived many observational tests and predictions. It is now widely accepted that the unified models are broadly correct at least to 'first order' (e.g. Antonucci 1993) and that many if not most type-2 AGN contain obscured type-1 nuclei.

An important corollary of the unified models is the expectation that populations of obscured (i.e. type 2) AGN will be present for all redshifts. These predicted populations are in general extremely difficult to identify observationally (e.g. Halpern & Moran 1998) except locally in low-luminosity AGN, and at high redshift ($0 < z \lesssim 5$) in the radio-loud AGN minority. Nevertheless, the strength and shape of the X-ray background has been taken as evidence of the existence of a large population of obscured

quasars, outnumbering normal quasars by a factor of several (e.g. Comastri et al. 1995). Such a large population of obscured quasars may also explain the unexpectedly large population of local remnant black holes (Fabian & Iwasawa 1999; Lawrence 1999). Even hard X-ray samples may miss the very heavily obscured objects, so an infrared-selected sample is the only reliable way to obtain a complete census of AGN. For example, it will be possible with ELAIS to make quantitative constraints on the dust distribution and torus column densities, as well as on the evolution of obscured quasar activity.

2.4 Dust in normal galaxies to cosmological distances

At the longer *ISO* wavelengths (90 and 175 μm) emission from the cool interstellar 'cirrus' dust in normal galaxies will be detectable in our survey in fainter and cooler objects than were accessible to *IRAS*. This will allow us to examine the temperature distribution functions and in particular look for unusually cool galaxies. Quantifying the distributions of such cool sources will be important for deep submillimetre (submm) surveys as there is considerable degeneracy between cool, low redshift and warm high redshift objects in this wavelength regime.

2.5 Circumstellar dust emission from galactic halo stars

We expect to detect hundreds of stars at 6.7 and 15 μm and it will be of interest to check whether any show evidence of an infrared excess because of the presence of a circumstellar dust shell. Such shells are expected from late type stars owing to mass loss while on the red giant branch, from cometary clouds or from proto-planetary discs. At the high galactic latitudes of our survey, late type stars with circumstellar dust shells should be rare (e.g. Rowan-Robinson & Harris 1983), so any detections of such shells could be especially interesting.

2.6 New classes of galactic and extragalactic objects

F10214+4724 (Rowan-Robinson et al. 1991a) was at the limit of *IRAS* sensitivity and new classes of objects may well be discovered at the limit of the ELAIS sensitivity. The lensing phenomenon which made F10214+4724 detectable by *IRAS* may become more prevalent at fainter fluxes, increasing the proportion of interesting objects.

2.7 The extragalactic background

The discovery of the 140–850 μm far-infrared background (Puget et al. 1996; Fixsen et al. 1998; Hauser et al. 1998; Lagache et al. 1998) from *COBE* data has shown that most of the light produced by extragalactic objects has been reprocessed by dust and re-emitted in the far-infrared and submm. This discovery provides further strong motivation for studying the dust emission from objects at all redshifts and all far-infrared wavelengths. It is possible to explain this far-infrared background radiation with a number of evolution models that are consistent with the *IRAS* data. The constraints provided by *ISO* surveys such as ELAIS are expected to be able to rule out some of these a priori models. The motivation behind our 175-μm survey was specifically to start to resolve this far-infrared background into its constituent galaxies.

3 SURVEY DEFINITION

3.1 Selection of survey wavelengths and area

In order to detect as many sources as efficiently as possible we restricted ourselves to two primary *ISO* broad-band filters and aimed to cover as large an area as possible. We selected filters with central wavelengths at: 15 μm (ISOCAM, Cesarsky et al. 1996), which is particularly sensitive to AGN emission, and 90 μm (ISOPHOT, Lemke et al. 1996), which is sensitive to emission from star-formation regions. At 90 μm we aimed to reach the confusion limit and pre-flight sensitivity estimates led us to conclude that this could be achieved with an on-sky integration time of 20 s. We decided to map the same area of sky at 15 μm using a similar total observation time and this required on-sky integration times of 40 s. In both cases these integration times were close to the minimum practical. A survey area of order 10 deg^2 was chosen to produce a statistically meaningful sample of galaxies. This area and depth was ideal to complement the deep ISOCAM surveys (Cesarsky et al. 1996; Taniguchi et al. 1997a; Elbaz et al. 1999) as discussed in Section 6.

A further justification for a large-area survey is that many of the sources will be at relatively low redshift (e.g. an ultra-luminous starburst would be detectable at $z = 0.5$ as discussed in Section 2.2). Thus, unless our survey is of a sufficient area, the volume will be such that cosmic variance can be a significant problem, i.e. large-scale clustering means that the mean density within a survey volume may not be representative of the universal mean. To estimate this effect we use the galaxy power spectrum as compiled by Peacock & Dodds (1994). From this we can estimate the variance in a survey of any given volume (we assume a cubical geometry, which means we will underestimate the variance). Fig. 5 illustrates the area required to study populations out to a given redshift allowing for different amounts of cosmic variance. From this we can see that a survey of around 10 deg^2 is required to measure the mean density of populations visible to $z = 0.5$ with negligible errors (<10 per cent) owing to large-scale structure. A survey with the area of ELAIS can also measure the mean density of populations $z = 0.25$ with 20 per cent accuracy. Populations below $z = 0.15$ would only have mean densities known to around

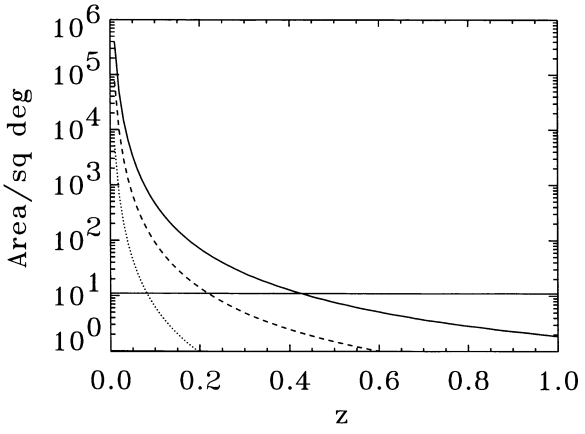

Figure 5. The minimum area of a survey required to measure mean densities in populations visible to a given redshift such that the systematic errors owing to large-scale structure are: $\sigma = 0.1$ – solid line, $\sigma = 0.2$ – dashed line and $\sigma = 0.5$ – dotted line. The nominal area of the ELAIS survey is over-plotted. This plot assumes that the survey area is split into four independent survey areas as is the case for ELAIS.

50 per cent. Fig. 6 shows what fractional errors we would expect in mean quantities derived from ELAIS for populations that are visible to different depths.

During the mission we introduced two additional filters. The first of these was designed to provide constraints on the infrared spectral energy distribution of ELAIS sources from fields (around 6 deg^2) that would not have been observed in time for pointed *ISO* follow-up. For this aspect of the survey we selected the 6.7-μm filter, which was the most sensitive for sources detected at 15 μm. Naturally, as well as providing improved spectral coverage of other ELAIS sources, this also produced an independent source list which was sensitive to emission from normal galaxies. The second filter, centred at 175 μm, was introduced specifically to explore the populations making up the far-infrared background as discussed in Section 2.7.

A more detailed description of the survey parameters is given Section 3.4.

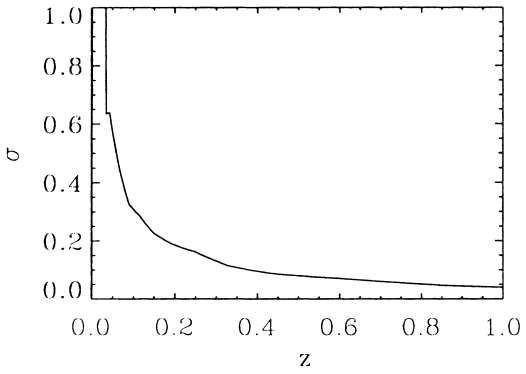

Figure 6. The fractional error in the mean densities resulting from cosmic variance for populations visible to a given redshift for the ELAIS survey.

Table 2. Summary of the total time spent by *ISO* on the ELAIS programme. This table is broken down into observations preformed for the survey (including reliability observations, calibration measurements and small fields) and the photometry section of the programme. Data flagged as 'aborted' or 'failed' by the *ISO* ground station are also singled out, however we have not experienced any problems with the 'aborted' data.

Category	Time/h	Number of AOTs
Awarded	377	
Survey (Observed)	324	174
Survey (Aborted)	7	3
Survey (Failed)	5	3
Photometry (Observed)	44	930
Total (Observed)	368	1104
Total (Observed & Aborted)	375	1107

3.2 Time awarded

Over the course of the *ISO* mission the ELAIS programme was awarded a total of 377 h. This allocation was used not only to perform the basic blank field survey observations, discussed in Section 3.1, but also a number of other related programmes.

Principal among these was an *ISO* photometry programme to investigate around 200 sources that had been detected by ELAIS in the early parts of the mission. These observations were designed to provide constraints on the spectral energy distributions of the ELAIS sources but would also provide a serendipitous, although biased, survey in their own right. In addition we were awarded time to observe a number of subfields repeatedly to help quantify our reliability and completeness. We also performed eight ISOPHOT calibration measurements on three known stars and three ELAIS sources, independently of the instrument team.

The amount of time actually spent and astronomical observation templates (AOTs) used on both the survey proper and the photometry programmes are summarized in Table 2.

3.3 Field selection

The allocated observing time was sufficient to observe around 12 deg^2. The choice of where to distribute the ELAIS rasters on the sky was governed by a number of factors. Firstly, we decided not to group these all in a single contiguous region of the sky; this further reduces the impact of cosmic variance on the survey (see Section 3.1). Distributing the survey areas across the sky also has advantages for scheduling follow-up work. Cirrus confusion is a particular problem, so we selected regions with low *IRAS*100-μm intensities ($I_{100} < 1.5$ MJy sr^{-1}), using the maps of Rowan-Robinson et al. (1991b). In recognition of the large amount of

Table 3. Summary of ELAIS survey fields. These fields were selected primarily for having low Cirrus contamination, specifically $I_{100} < 1.5$ MJy sr^{-1} from the *IRAS* maps of Rowan-Robinson et al. (1991b); the I_{100} quoted in this table are from the maps of Schlegel et al. (1998). For N1–3, S1 and all X fields we also restricted ourselves to regions of high visibility >25 per cent over the mission lifetime. For low zodiacal background we required $|\beta| > 40$ and to avoid saturation of the ISOCAM detectors we had to avoid any bright *IRAS* 12-μm sources. Approximate dimensions of the fields in degrees ($X \times Y$) are given along with the orientation from north to the Y axis eastwards in degrees (ROLL). The six smaller rasters X1–6 are centred on well-studied areas of the sky or high-z objects.

Name	Nominal coordinates J2000		X /°	Y /°	ROLL /°	$\langle I_{100}\rangle$ /Mjysr^{-1}	Visibility /per cent	β
N1	$16^h10^m01^s$	$+54°30'36''$	2.0	1.3	76	0.43	98	73
N2	$16^h36^m58^s$	$+41°15'43''$	2.0	1.3	59	0.40	59	62
N3	$14^h29^m06^s$	$+33°06'00''$	2.0	1.3	110	0.48	27	45
S1	$00^h34^m44^s$	$-43°28'12''$	2.0	2.0	77	0.37	32	−43
S2	$05^h02^m24^s$	$-30°35'55''$	0.3	0.3	290	0.55	32	−43
X1 (Phoenix)	$01^h13^m13^s$	$-45°14'07''$	0.4	0.4	33	0.62	36	−48
X2 (Lockman 3)	$13^h34^m36^s$	$+37°54'36''$	0.4	0.4	280	0.28	17	44
X3 (Sculptor)	$00^h22^m48^s$	$-30°06'30''$	0.4	0.4	254	0.99	28	−30
X4 (VLA 8)	$17^h14^m14^s$	$+50°15'24''$	0.3	0.3	162	0.87	99	73
X5 (TX0211-122)	$02^h14^m17^s$	$-11°58'46''$	0.3	0.3	254	1.22		−65
X6 (TX1436+157)	$14^h36^m43^s$	$+15°44'13''$	0.3	0.3	124	1.19	22	29

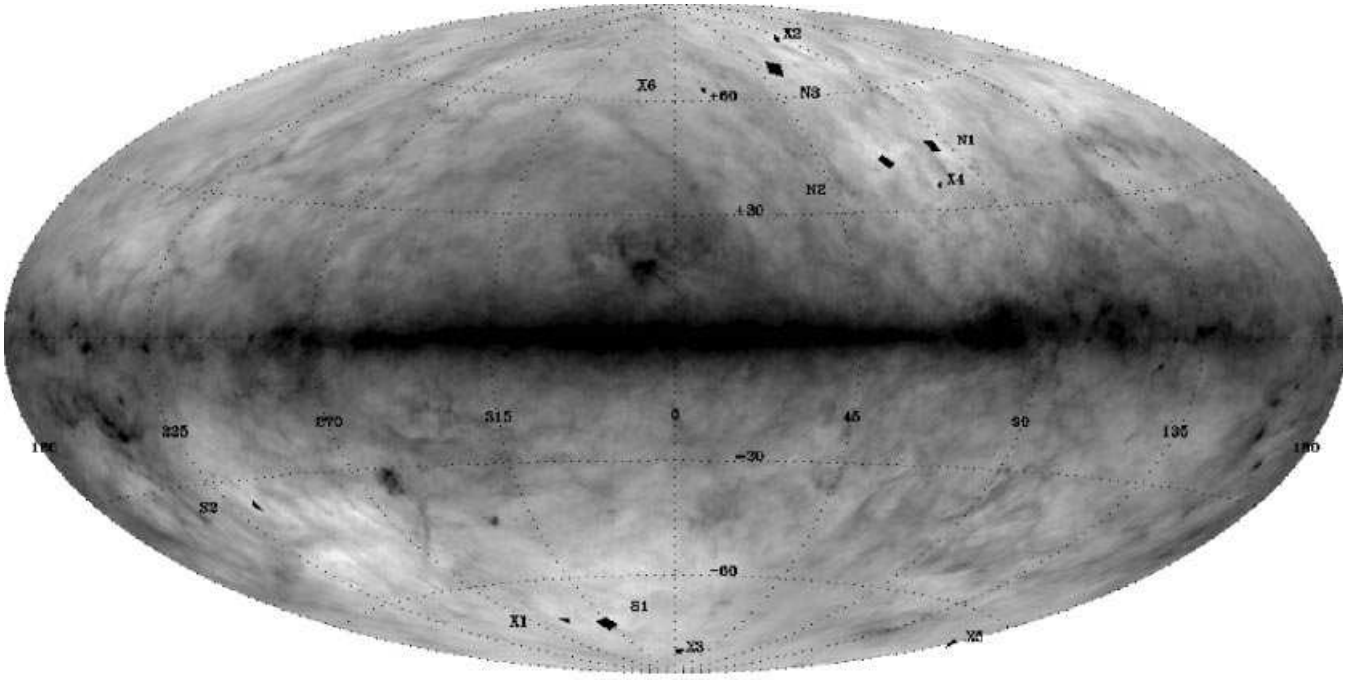

Figure 7. The location of the ELAIS survey fields overlaid on a Hammer–Aitoff equal area projection of the *COBE* normalized *IRAS* maps of Schlegel et al. (1998). Galactic latitude and longitude gridlines are overlaid.

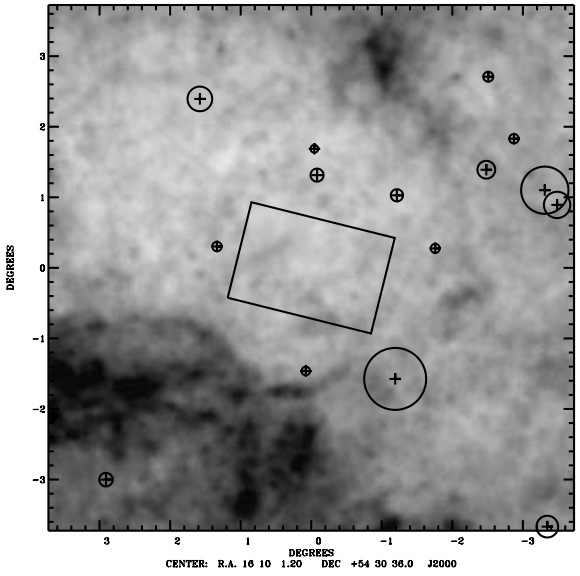

Figure 8. The location of the N1 ELAIS survey field overlaid on the *COBE* normalized *IRAS* maps of Schlegel et al. (1998). *IRAS* sources with 12-μm fluxes brighter than 0.6 Jy are overlayed with radius proportional to flux for $S_{60} < 10$ Jy. The minimum 100-μm intensity shown is 0 MJy sr^{-1} (white) and the maximum is 1.5 MJy sr^{-1} (black).

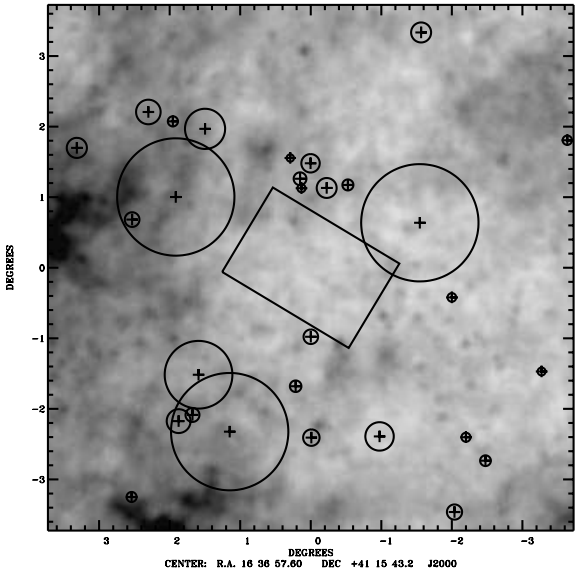

Figure 9. The location of the N2 ELAIS survey field overlaid on the *COBE* normalized *IRAS* maps of Schlegel et al. (1998). *IRAS* sources with 12-μm fluxes brighter than 0.6 Jy are overlayed with radius proportional to flux for $S_{60} < 10$ Jy. The minimum 100-μm intensity shown is 0 MJy sr^{-1} (white) and the maximum is 1.5 MJy sr^{-1} (black).

time required we decided to minimize scheduling conflict with other *ISO* observations by further restricting ourselves to regions of high visibility (>25 per cent) over the mission lifetime, while to reduce the impact of the zodiacal background we only selected regions with high ecliptic latitudes ($|\beta| > 40°$). Finally, it was essential to avoid saturation of the ISOCAM detectors, so we had to avoid any bright *IRAS* 12-μm sources ($S_{12} > 0.6$ Jy). These requirements led us to selecting the four main fields detailed in the upper portion of Table 3. The location of all ELAIS fields are indicated in Fig. 7 showing the Galactic Cirrus distribution, while in Figs 8–11 we show the nominal boundaries of each of the main survey fields overlayed on a Cirrus map.

Towards the end of the mission an additional field (S2) was selected with similar criteria; this field was multiply observed to provide reliability and completeness estimates.

A further six fields were selected as being of particular interest to warrant a single small (24×24 arcmin^2) raster. These were chosen either because of existing survey data or because the field contained a high redshift object and were thus more likely to contain high redshift *ISO* sources.

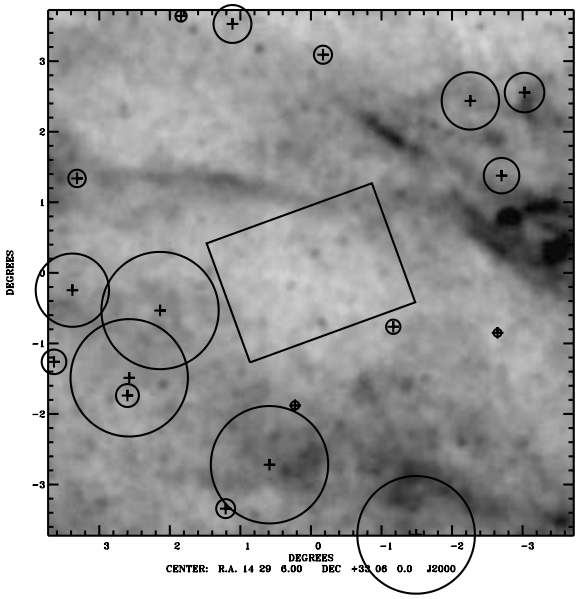

Figure 10. The location of the N3 ELAIS survey field overlaid on the *COBE* normalized *IRAS* maps of Schlegel et al. (1998). *IRAS* sources with 12-μm fluxes brighter than 0.6 Jy are overlayed with radius proportional to flux for $S_{60} < 10$ Jy. The minimum 100-μm intensity shown is 0 MJy sr^{-1} (white) and the maximum is 1.5 MJy sr^{-1} (black).

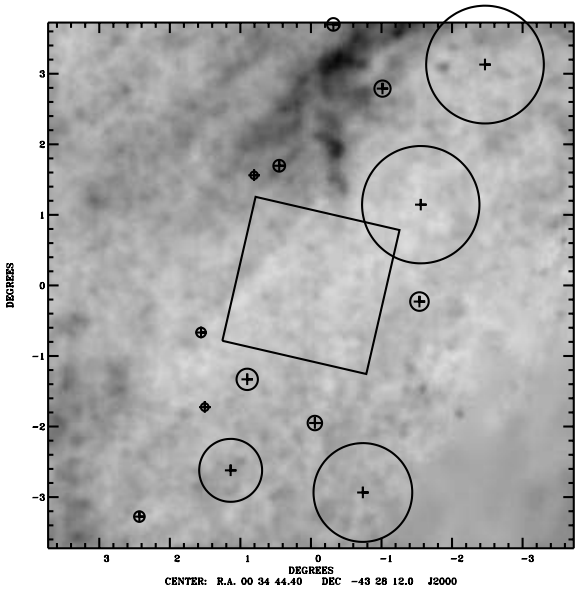

Figure 11. The location of the S1 ELAIS survey field overlaid on the *COBE* normalized *IRAS* maps of Schlegel et al. (1998). *IRAS* sources with 12-μm fluxes brighter than 0.6 Jy are overlayed with radius proportional to flux for $S_{60} < 10$ Jy. The minimum 100-μm intensity shown is 0 MJy sr^{-1} (white) and the maximum is 1.5 MJy sr^{-1} (black).

(i) **Phoenix.** This field was the target of a deep radio survey (Hopkins et al. 1998) and has been extensively followed up from the ground with imaging and spectroscopy.

(ii) **Lockman 3.** This was one of the deep *ROSAT* survey fields (McHardy et al. 1998).

(iii) **Sculptor.** This field has been the subject of an extensive ground-based optical survey programme (e.g. Galaz & De Lapparent 1998).

Table 4. Summary of the AOT parameters for the bulk of survey programme observations. The 90-μm survey strategy changed after the S1 and N1 observations, and the revised parameters are illustrated. Many observations in N3 and all of the smaller fields X1–6 and S2 were executed with very similar AOTs, but with fewer pointings. Parameters are described in the text and in detail on the *ISO* WWW pages (http://isowww.estec.esa.nl/).

	ISOCAM		ISOPHOT	
Parameter				
Detector	LW	LW	C100	C200
Filter	LW2	LW3	C90	C160
λ/μm	6.75	15	95.1	174
$\Delta\lambda$/μm	3.5	6	51.4	89.4
Gain	2	2	n/a	n/a
TINT/s	2	2	20 12	32
NEXP	10	10	n/a	n/a
NSTAB	80	80	n/a	n/a
PFOV/arcsec	6	6	43.5	84.5
NPIX	32	32	3	2
M, *N*	28, 14	28, 14	10, 20 20, 20	13, 13
d*M*, d*N*/arcsec	90, 180	90, 180	130, 130 75, 130	96, 96

(iv) **VLA 8.** This field is centred on a $z = 2.394$ radio galaxy (Windhorst et al. 1991) and has been the target of a deep *Hubble Space Telescope* observations (Windhorst, Keel & Pascarelle 1998).

(v) **TX0211-122.** This object is at $z = 2.34$ (van Ojik et al. 1994) and was discovered in the Texas radio survey (Douglas et al. 1996).

(vi) **TX1436+157.** This object is at $z = 2.538$ (Röettgering et al. 1997) and was discovered in the Texas radio survey (Douglas et al. 1996). The *ISO* field centre is offset from the radio object as the B1950 equinox coordinates were entered rather than the J2000 coordinates.

These six regions are also described in the lower portion of Table 3.

3.4 Observation parameters

Table 4 summarizes the instrument parameters specified in the majority of our survey AOTs. Most are self explanatory.

For ISOCAM the Gain was set to 2 which was the standard used for most ISOCAM observations. TINT was the integration time per readout and NEXP was the number of readouts per pointings (i.e. the total integration time per pointing is NEXP × TINT). NSTAB was the additional number of readouts for the first pointing of a raster added to allow the detector to stabilize.

With ISOPHOT, TINT was the total integration time per pointing.

The parameters related to the raster geometry (PFOV, NPIX, *M*, *N*, d*M*, d*N*) have the same meaning for each instrument. PFOV is the nominal pixel field of view on the sky. NPIX is the number of pixels along each axis of the detector array. *M*,*N* are the number of steps in a raster while d*M*, d*N* are the step sizes.

The ISOCAM rasters were designed such that each sky position was observed twice in successive pointings to improve reliability. To reduce overheads we selected a very large raster size, 40×40 arcmin^2. With the exception of small rasters and one test raster, the ISOCAM parameters remained unchanged throughout the survey.

Since the ISOPHOT internal calibration measurements were only performed at the beginning and end of a raster we chose these

to be half the size of the ISOCAM rasters (20×40 arcmin^2). We originally used ISOPHOT with a non-overlapping raster pattern and switched to an overlapping mode during the mission, with most N1 and S1 observations performed in the non-overlapping mode.

The observation parameters for all survey observations are tabulated in Appendix A.

4 *ISO* OBSERVATIONS

The *ISO* observations for the ELAIS programme were executed from 1996 March 12 (revolution 116), 37 d after the beginning of routine operations (1996 February 4, revolution 79) until 17:44 on 1998 April 8 (revolution 875), 10 h 44 min after the first signs of boil off had been detected and 5 h 23 min before the last observations were performed.

In general the execution of the planned observations was very successful. Only three observations were reported as 'failed'. Three observations were flagged as 'aborted', all three of these had been concatenated to 'failed' observations but appear to have been successfully executed despite this.

The only significant problem in the execution of the survey observations occurred in N3. It transpired that there was a paucity of guide stars in this region and the mission planning team were unable to schedule many of the observations near the original dates requested. To accommodate this problem the sizes of the rasters were reduced and restrictions on the possible observation dates relaxed. However, in the last available observing window for N3 other *ISO* mission priorities, together with remaining guide star acquisition problems, interfered with the scheduling. The net result is that the coverage of the N3 region is patchy.

It may be that this guide star problems noticed in N3 may be related to an apparent offset of around 6 arcsec between the reference frame of the DSS and e.g. the APM catalogue in this field. The APM catalogue agrees very well with the Guide Star Catalogue v1.2 (`http://www-gsss.stsci.edu/gsc/gsc12/gsc12_form.html`).

Table 5. Survey fields covered at least once. Areas are given in deg^2.

Field	Wavelength/μm			
	6.7	15	90	175
N1		2.67	2.56	2[a]
N2	2.67	2.67	2.67	1
N3	1.32	0.88	1.76	
S1	1.76	3.96	3.96	
S2	0.12	0.12	0.11	0.11
X1		0.16	0.19	
X2		0.16	0.19	
X3		0.16	0.19	
	5.87	10.78	11.63	3.11
X4		0.09	0.11	
X5		0.09		
X6		0.09	0.11	

[a] The 175-μm observations in N1 have been carried out by the FIRBACK team (PI J-L Puget, see Dole et al. 1999) and are included in this table to illustrate the complete *ISO* coverage of the ELAIS fields. N1–3, S1–2 and X1–3 are unbiased survey fields, while X4–6 are centred on known objects so should not be included with the other fields for statistical purposes.

4.1 Main survey observations

Table 5 indicates the area that has been surveyed at least once in any band in all of our fields. For the four large fields the separation of the raster pointings (40 arcmin) is used to compute the area, i.e. 0.44 deg^2 per raster. For the small fields which are not mosaiced the actual size of the raster is used.

The coverage, in terms of integration time per sky pixel, of the four main survey fields (N1–3 and S1) in each of the bands are shown in Figs 12–15.

4.2 Duplicate survey observations

A number of subfields have been repeated on one or more occasions. This repetition will considerably aid in assessing the reliability and completeness of the survey. In addition this data will provide deeper survey regions which are good targets for more focused follow-up campaigns and other exploitation.

Table 6 lists all the fields that have repeated observations together with the level of redundancy.

4.3 Photometry programme

In addition to the survey observations, we also undertook a photometry programme to observe objects detected early on in the survey programme at other *ISO* wavelengths.

These objects were selected from the S1 and N1 survey regions which had been observed at an early stage in the campaign. 180 objects, which had been detected at 15 μm, were selected to be observed with ISOCAM at 4.5, 6.7, 9 and 11 μm using the filters LW-1, LW-2, LW-4 and LW-7. 80 objects were selected to be observed by ISOPHOT at 60 and 175 μm, using the C60 and C160 filters.

The ISOCAM observations were performed in concatenated chains of 10 pointings. At each pointing a 2×1 raster was performed to ensure accurate photometry and reliable detections. The chains were arranged such that each of the 10 sources was located in a different position on the array (separated by around 18 arcsec), this was to allow accurate sky flat-fielding over the course of the concatenated chain. The 120 ISOCAM pointings in S1 and the 80 pointings in N1 were ordered to minimize the total path length, ensuring that sequential observations were as close to each other as possible, both spatially and temporally, improving the flat-fielding.

The ISOPHOT observations were performed in chains of 15 pointings. On average the 15 pointings contained five source positions and 10 background positions. Like the ISOCAM photometry observations, the ISOPHOT source positions were ordered to minimize the total path length. The background pointings were chosen to be spaced along this path at reasonably regular intervals, while ensuring that there was at least one background position between every source position.

Other parameters from the AOTs for the photometry programme are summarized in Table 7.

5 DATA PROCESSING AND PRODUCTS

In order to provide targets early on in the campaign to allow follow-up programmes, both from the ground and with *ISO*, it was decided to perform an initial 'preliminary analysis'. This was started long before the end of the mission, while the understanding

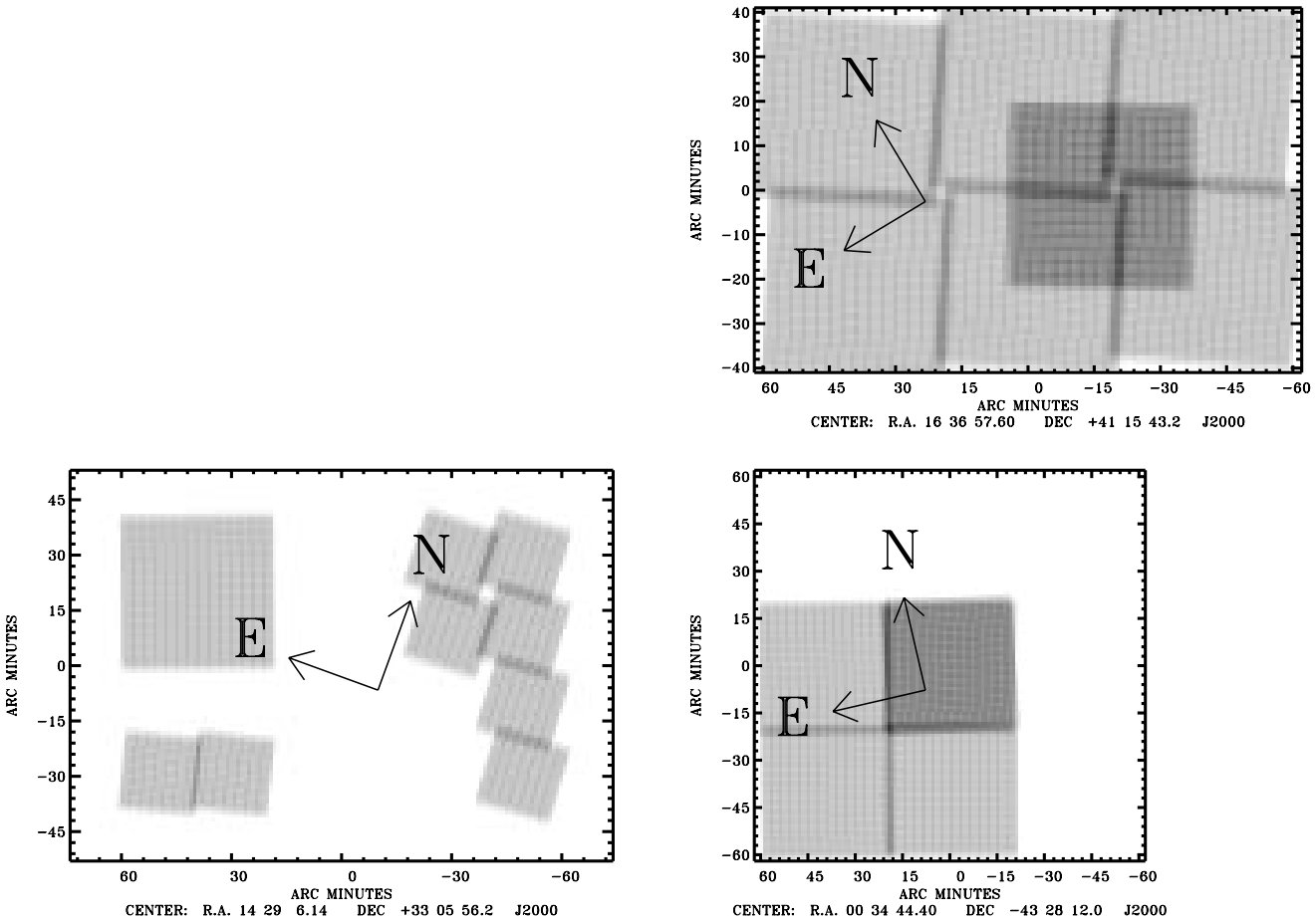

Figure 12. Survey coverage at 6.7 μm. White areas have not been covered at all; darker regions indicate longer total integration, either because of repeated observations or overlap, black indicates 200 s. The coverage maps have been smoothed to 1 arcmin resolution. Reading from top left to bottom right the fields are: N2, N3, S1. The true peaks in the coverage are around 150, 100 and 175 s respectively.

of the behaviour of the instruments was naturally less than it is currently and will be superseded with a 'final analysis' incorporating the best available knowledge post-mission.

The preliminary analysis was conducted with the intention of producing reliable source lists at 6.7, 15 and 90 μm. The processing of the ISOCAM survey observations is described in detail by Serjeant et al. (2000) and the reduction of the ISOPHOT 90-μm survey data will be discussed by Efstathiou et al. (2000).

The final analysis is currently being undertaken. This is expected to produce better calibrated and fainter source lists than the preliminary analysis. The final analysis will also produce maps which can be used to determine fluxes or upper limits for known sources. This analysis will not, however, be completed until early 2000.

The ELAIS products will comprise source catalogues at all wavelengths, 4.5, 6.7, 9, 11, 15, 60, 90, 175, together with maps from all the survey observations. Highly reliable subsets of the 'preliminary analysis' catalogues were released to the community, via our WWW site (`http://athena.ph.ic.ac.uk/`), concurrent with the expiration of the propriety period on 1999 August 10.

5.1 Data quality

The quality of the 15-μm ISOCAM data is moderately uniform. Some rasters are more affected by cosmic rays than others but the total amount of data seriously affected by cosmic rays is small. The noise levels are within a factor of a few of those expected; a typical noise level is $0.2\,\mathrm{ADU\,s^{-1}\,pixel^{-1}}$ per pointing.

The ISOPHOT data is seriously affected by cosmic rays and detector drifts. We have used the fluctuations in the time sequence of each pixel as an estimate of the average noise level. The fluctuations per pointing were typically 3 per cent of the background level, although three of the nine pixels were noisier with fluctuations typically 4 per cent of the background. A few observations showed higher noise as a result of the increased cosmic ray hits. Our original AOTs employed an integration time of 20 s. We subsequently decreased this to 12 s to allow for an overlapping raster giving a factor of 2 redundancy with similar observation time. Importantly there does not appear to be a significant difference in noise levels per pointing despite the factor of 2 reduction in integration time, indicating that non-white noise in the pixel histories is dominant. The redundancy introduced by this new strategy could improve the signal-to-noise ratio for sources by as much as $\sqrt{2}$.

5.2 Preliminary data analysis

The processing for the ISOPHOT and ISOCAM data proceeds in a similar fashion. All data reduction used a combination of standard

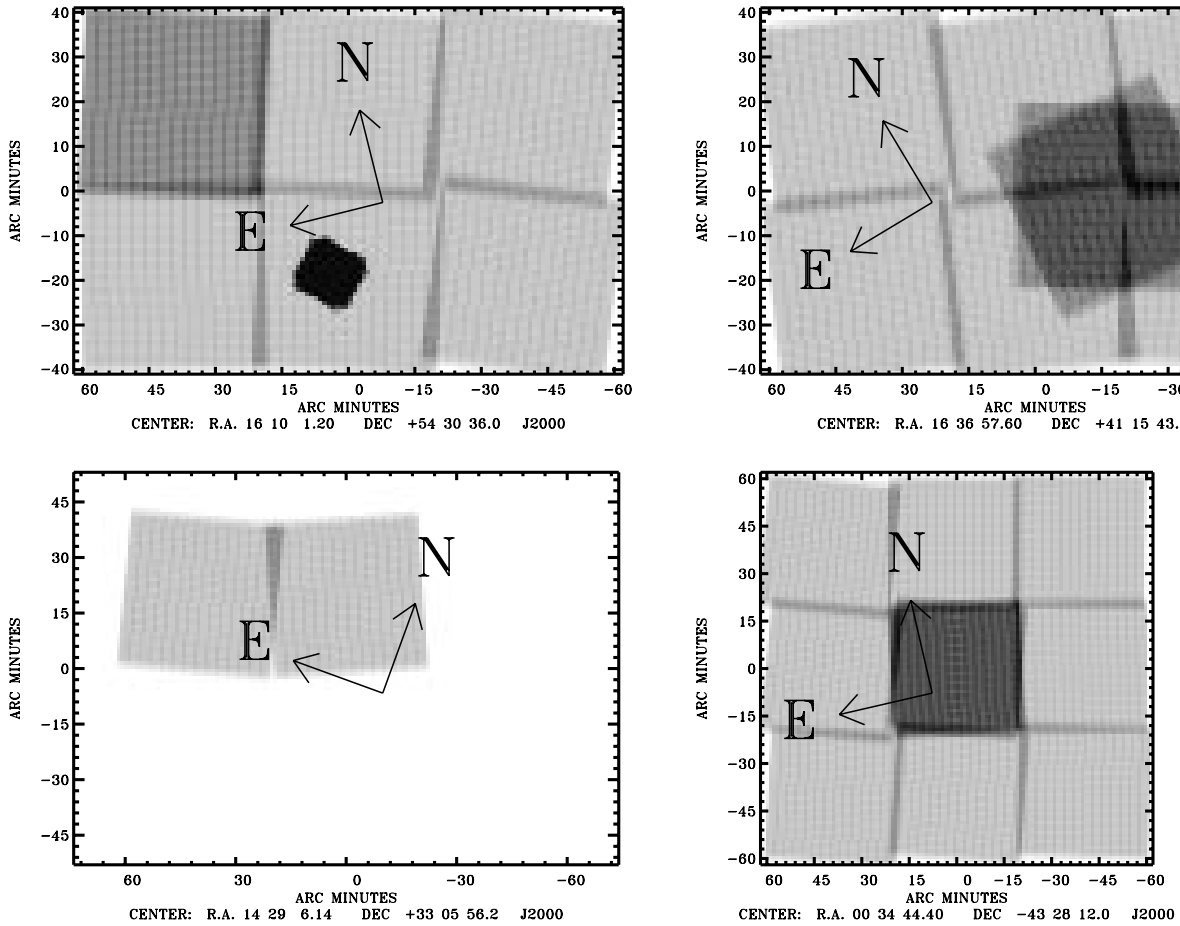

Figure 13. Survey coverage at 15 μm. White areas have not been covered at all; darker regions indicate longer total integration, either because of repeated observations or overlap, black indicates 200 s. The coverage maps have been smoothed to 1 arcmin resolution. Reading from top left to bottom right the fields are: N1, N2, N3, S1. The true peaks in the coverage are around 600, 200, 100 and 200 s respectively.

routines from the PHOT interactive analysis (PIA, Gabriel et al. 1996)[1] software and the CAM interactive analysis (CIA, Ott et al. 1998) together with purpose-built Interactive Data Language (IDL) routines. The frequency of glitches and other transient phenomena led to non-Gaussian and non-white-noise behaviour.

A number of data reduction techniques were tested at ICSTM, CEA/SACLAY, IAS and MPIA. Parallel pipeline processes for reducing the ISOPHOT data were run at both ICSTM and MPIA. Data reduction techniques suitable for ISOCAM data with multiple redundancy, such as the observations of the Hubble Deep Field (Serjeant et al. 1997), e.g. the Pattern Recognition Technique for ISOCAM data (Aussel et al. 1999) were unsuccessful in processing this data. The most reliable approach for source extraction was found to be that of looking for source profiles in the time histories of individual pixels rather than by constructing sky maps.

For both instruments the data stream from each detector pixel was treated as an independent scan of the sky. These data streams were filtered to remove glitches and transients and averaged to produce a single measurement at each pointing position. Significant outliers remaining in the data streams were flagged as potential sources. For the ISOCAM observations the redundancy of the pointings was used to provide confirmation of candidate sources. The data stream surrounding all remaining candidates was then examined independently by at least two observers to remove spurious detections. Sources that were acceptable to two or more observers were classified as good ($REL = 2$) and those acceptable to only one observer were classified as marginal ($REL = 3$).

The fraction of spurious detections was high as a result of the non-Gaussian nature of the noise and relatively low thresholds applied. More than 13 000 ISOPHOT source candidates were examined as were just over 15 000 ISOCAM 15-μm candidates. At 6.7 μm the rejected fraction was lower and the candidate list was only 3000. The final numbers of objects in the Preliminary Catalogue Version 1.3 are tabulated in Table 8.

The 'eye-balling' technique while laborious ensured that the resulting catalogues are highly reliable, as discussed in greater detail in Serjeant et al. (2000) and Efstathiou et al. (2000). The subsets of the Preliminary Catalogues that were released to the community were those ISOPHOT sources that had been confirmed by four observers, and those ISOCAM sources that had been confirmed by two observers with fluxes above 4 mJy, these subsets are exceptionally reliable.

A 'final analysis' process has been developed which uses the transient correction techniques of Lari (in preparation). These

[1] PIA is a joint development by the ESA Astrophysics Division and the ISOPHOT Consortium.

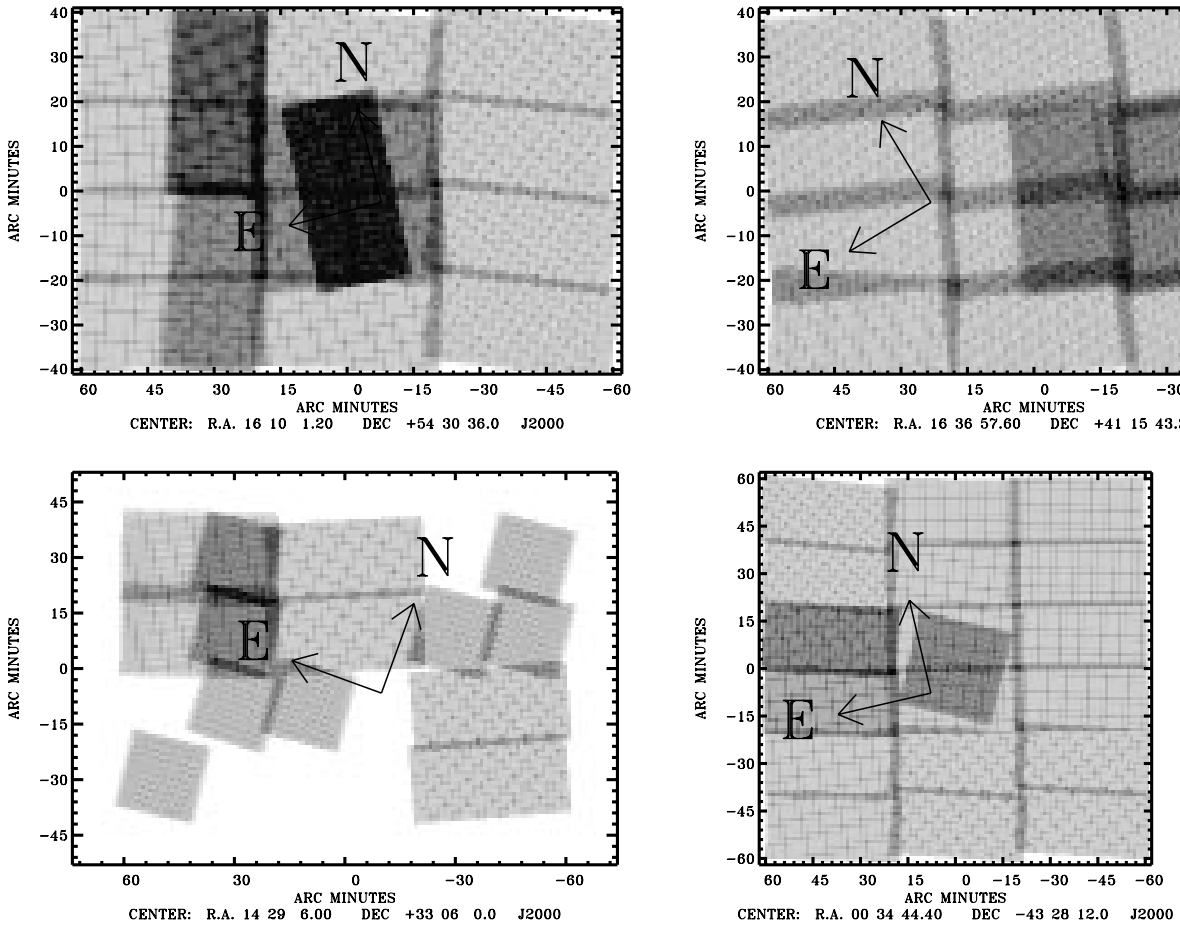

Figure 14. Survey coverage at 90 μm. White areas have not been covered at all; darker regions indicate longer total integration, either because of repeated observations or overlap, black indicates 100 s. The coverage maps have been smoothed to 1 arcmin resolution. Reading from top left to bottom right the fields are: N1, N2, N3, S1. The true peaks in the coverage are around 160, 120, 120 and 120 s respectively.

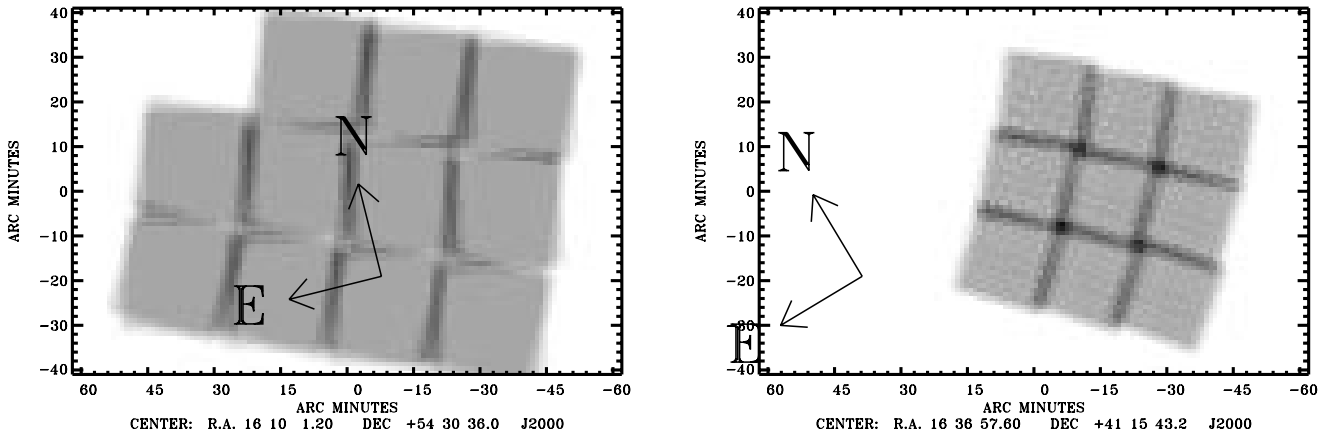

Figure 15. Survey coverage at 175 μm. NB Only the coverage in N2 is part of the ELAIS project, the coverage in N1 (left) comes from the FIRBACK team (PI J-L. Puget, see Dole et al. 1999). White areas have not been covered at all; darker regions indicate longer total integration, either because of repeated observations or overlap, black indicates 350 s. The coverage maps have been smoothed to 1 arcmin resolution. The true peaks in the coverage are around 260 and 350 s respectively.

techniques have been shown to be excellent for reducing ISOCAM data. While this is almost certainly the best procedure for reducing the ELAIS data, it is labour intensive and time consuming and we do not expect the 'final analysis' to be finished until early 2000, hence the release of our 'preliminary' products.

5.3 Source calibration

For the ISOCAM observations we have of order 10 stars per raster and these provide a very good calibration. A preliminary analysis of the star fluxes (Crockett et al., in preparation; see also Serjeant

Table 6. Survey subfields covered more than once, listing the area covered (in deg^2) and the number of times that subfield has been observed.

Field	Coordinates (J200)		Wavelength/μm			
			6.7	15	90	175
N1_T	$16^h10^m01^s$	$+54°30'36''$			0.22×3	2×2
					0.22×4	
N1_U	$16^h11^m00^s$	$+54°13'23''$		0.04×11		
N1_1C	$16^h13^m54^s$	$+54°18'22''$			0.22×2	
N_2	$16^h13^m57^s$	$+54°59'36''$	0.44×2			
N2	$16^h35^m45^s$	$+41°06'00''$	0.44×2	0.44×3	0.44×3	1×2
N3_5C/D	$14^h31^m53^s$	$+33°14'37''$		0.22×2		
S1_5	$00^h34^m44^s$	$-43°28'12''$	0.44×2	0.44×3	0.22×3	
S2	$05^h02^m24^s$	$-30°35'55''$		0.12×4	0.11×5	0.11×3

Table 7. Summary of the AOT parameters for the photometry programme.

Instrument	ISOCAM				ISOPHOT	
Parameter						
Detector	LW	LW	LW	LW	C100	C200
Filter	LW1	LW2	LW4	LW7	C60	C90
λ/μm	4.5	6.7	6.0	9.62	60.8	174
$\Delta\lambda$/μm	1	3.5	1	2.2	23.9	71.7
Gain	2	2	2	2	n/a	n/a
TINT/s	5	5	5	5	32	32
NEXP	8	8	8	8	n/a	n/a
NSTAB	50	50	50	50	n/a	n/a
PFOV/arcsec	6	6	6	6	43.5	84.5
M, *N*	2, 1	2, 1	2, 1	2, 1	1, 1	1, 1
d*M*, d*N*/arcsec	24	24	24	24	n/a	n/1

Table 8. ELAIS preliminary source catalogue statistics.

Quality	Wavelength/μm		
	6.7	15	90
Good (*REL* = 2)	795	728	153
Moderate (*REL* = 3)	2341	818	208

et al. 2000) suggests that our raw instrumental units (ADU g^{-1} s^{-1}) need to be multiplied by a factor of 1.75 to give fluxes in mJy. This implies a 50 per cent completeness limit of approximately 3 mJy at 15 μm. The flux calibration is still uncertain at 6.7 μm, largely because of the uncertain aperture corrections to the under-sampled observations and the single-pixel detection algorithm, although PSF models and pre-flight sensitivity estimates suggest a 50 per cent completeness level at less than 1 mJy. (See Serjeant et al. 2000 for more details.)

For the 90-μm survey the calibration proceeded as follows. The expected background was estimated using *COBE* and *IRAS* data and zodiacal light models. These predictions were compared to the measurements of the background calibrated using the internal calibration device (FCS) allowing the predicted backgrounds to be corrected from an extended source to a point-source calibration. These predictions were then used to scale the measured fluctuations above the background. Single pixel detections ('point sources') were then calibrated using the expected fraction of flux falling on a single pixel for a source placed arbitrarily with respect to the pixel centre. The fluxes of 'extended sources' were calculated in a more complicated fashion and have great associated uncertainties. The fluxes were found to be in good agreement with model stellar fluxes in our own dedicated calibration measurements and with the fluxes of *IRAS* sources in the fields. This suggests a 5σ noise level of 100 mJy. This ISOPHOT calibration, completeness and reliability estimate is discussed in detail by Efstathiou et al. (2000) and Surace et al. (in preparation).

6 COMPARISON WITH OTHER *ISO* SURVEYS

ISO carried out a variety of complementary surveys exploring the available parameter space of depth and area. Table 9 summarizes the main extragalactic blank-field surveys. With the exception of the two main serendipity surveys ELAIS covers the largest area and has produced the largest number of *ISO* sources. Fig. 16 illustrates how deeper smaller area surveys are complemented by shallower wider area surveys.

7 FOLLOW-UP

An extensive follow-up programme is being undertaken, including observations in many bands from X-ray to radio. This programme will provide essential information for identifying the types of objects detected in the infrared, their luminosities, energy budgets and other detailed properties. As well as studying the properties of the objects detected by *ISO* a number of the follow-up surveys will provide independent source lists which will be extremely valuable in their own right, e.g. to investigate the differences between infrared and non-infrared emitting objects.

7.1 Surveys

A number of follow-up programmes are in fact independent surveys at other wavelengths, carried out within the ELAIS survey area. These are summarized in Table 9 and include:

(i) **Optical:** *R*-band CCD surveys are essential to provide optical identifications for spectroscopic and related follow-up with improved astrometry, photometric accuracy and to fainter levels than those provided by the Second Sky Survey. Our principal southern field (S1) has been completely covered with the ESO/Danish 1.5-m telescope to a depth of $R \sim 23.5$ (La Franca et al., in preparation), while all our northern fields N1–3 have been completed to a similar depth using the Isaac Newton Telescope (INT) Wide Field Camera (Verma et al., in preparation). Other optical bands allow object classification and other more detailed investigations. Four square degrees within our northern fields have been observed to a depth of $U \sim 22$ (Verma et al., in preparation). In 1999 June, we observed the central 1.2 deg^2 of S1 in *U* and

Table 9. Field surveys with *ISO*, ordered roughly in decreasing area.

Survey name	E.g. reference	Wavelength /μm	Integration /s	Area /deg^2
PHT Serendipity Survey	1	175	0.5	7000
CAM Parallel Mode	2	6.7	150	33
ELAIS	3	6.7, 15, 90, 175	40, 40, 24, 128	6, 11, 12,1
CAM Shallow	4	15	180	1.3
FIRBACK	5	175	256, 128	1, 3
IR Back	6	90, 135, 180	23, 27, 27	1, 1, 1
SA 57	6.7	60, 90	150, 50	0.42, 0.42
CAM Deep	8	6.7, 15, 90	800, 990, 144	0.28, 0.28, 0.28
Comet fields	9	12	302	0.11
CFRS	10	6.7, 15, 60, 90	720, 1000, 3000, 3000	0.067.0.067.0.067, 0.067
CAM Ultra-Deep	11	6.7	3520	0.013
ISOHDF South	12	6.7, 15	>6400, >6400	4.7e-3, 4.7e-3
Deep SSA13	13	6.7	34000	2.5e-3
Deep Lockman	14, 15	6.7, 90, 175	44640, 48, 128	2.5e-3, 1.2, 1
ISOHDF North	15	6.7, 15	12800, 6400	1.4e-3, 4.2e-3

References: 1 – Bogun et al. (1996), 2 – Siebenmorgen et al. (1996), 3 – this paper, 4 – Elbaz et al. (1999), 5 – Dole et al. (1999), 6 – Mattila et al. (in preparation), 7 – Linden-Vørnle (1997), 8 – Elbaz et al. (1999) 9 – Clements et al. (1999), 10 – Flores et al. (1999a,b), 11 – Elbaz et al. (1999), 12 – Oliver et al. (in preparation), 13 – Taniguchi et al. (1997a), 14 – Taniguchi et al. (1997b), 15 – Kawara et al. (1998), 16 – Serjeant et al. (1997).

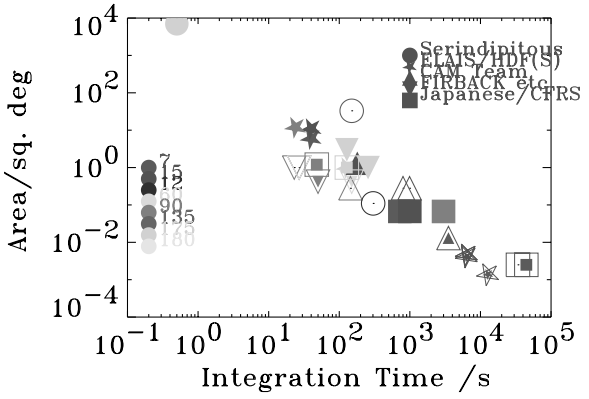

Figure 16. Figure comparing *ISO* survey area versus depth. All the surveys in Table 9 are plotted. The ELAIS points have an additional outline.

3 deg^2 in *I* using the European Space Agency (ESO) Wide Field Imager (Héraudeau et al., in preparation) and with these we expect to reach $U \sim 23$, $I \sim 23$. McMahon et al. (`http://www.ast.cam.ac.uk/~rgm/int_sur/`) have covered around 9 deg^2 of N1 to $u \sim 23.3$, $g \sim 24.2$, $r \sim 23.5$, $i \sim 22.7$, $z \sim 21.1$ and 2 deg^2 in N2 to similar depths in *g*, *r*, *i*, *z* as part of the INT wide field survey. The *U*-band surveys will be especially interesting as they will allow us to compute the *U*-band luminosity density (and hence star-formation rate) in the same volume as we calculate the infrared luminosity density, providing a direct comparison between obscured and unobscured star formation estimators.

(ii) **Near-infrared:** A substantial area has been surveyed in the near-infrared. In the *H*-band, around 0.85 deg^2 in N1 and N2 was surveyed using CIRSI on the INT (Gonzalez-Solares et al., in preparation). Approximately 0.5 deg^2 has been surveyed in both N1 and N2 in K' using Omega Prime on the Calar Alto 3.5 m (Rigopoulou et al., in preparation). The smaller, multiply repeated southern field S2 has been covered in *K* with SOFI on the NTT (Héraudeau et al., in preparation).

(iii) **Radio:** 21-cm radio data at sub-mJy level will allow identification of some of the most interesting objects which are expected to be very faint in the optical but would have detectable radio fluxes if they obey the usual radio to far-infrared correlation. These surveys will also allow an independent estimate of the star-formation rate within the same volume. The southern field S1 is completely covered to a depth of 0.3 mJy (Gruppioni et al. 1999b), and the 6 deg^2 in the northern fields has been covered to a depth of 0.2 mJy (Ciliegi et al. 1999). A deeper survey in the south has been conducted on the smaller, multiply repeated field S2 (Gruppioni et al., in preparation).

(iv) **X-ray:** Almaini et al. have been awarded 150 ks to do two deep *Chandra* pointings one in N1 and one in N2. La Franca et al. have also been awarded 200 ks on *BeppoSAX* to make five pointings covering around 2 deg^2 in S1.

(v) **Sub-mm:** The UK SCUBA Survey Consortium (Rowan-Robinson et al., independent of ELAIS) are performing part of their shallow (8 mJy) 850-μm survey in N1 and N2 and are aiming to cover 200 arcmin^2 in each.

Additional multi-wavelength surveys of these fields are expected in the near future.

7.2 Photometry and spectroscopy

We intend to obtain spectroscopic identifications for all (or the vast majority) of optical candidates for all ELAIS sources. This involves a two-pronged attack using multi-object spectroscopy for the brightest objects and single object spectroscopy using 4-m class telescopes on the fainter objects. This will be principally to obtain the redshifts and thus luminosity but also for classification and to assess star-formation rates. Some preliminary multi-fibre spectroscopy has been carried out with FLAIR on the UK Schmidt Telescope. This been supplemented by single object spectroscopy from the ESO/Danish 1.5-m telescope to provide spectroscopy on a complete sample of 90-μm selected sources (Linden-Vørnle et al., in preparation). A further 100 sources have been identified spectroscopically in a largely weathered-out run on the 2dF in 1998 September (Gruppioni et al., in preparation) and an additional night on the 2dF in 1999 August was also seriously hampered by weather (Oliver et al., in preparation). 40 spectra for fainter sources have already been taken with EMMI on the NTT and EFOSC2 on the ESO 3.6-m Telescope (La Franca et al., in preparation).

Table 10. Multi-wavelength field surveys within the main ELAIS fields, the vast majority carried out as part of the ELAIS collaboration. Areas are in deg^2. Some subfields within these go to greater depth. The X-ray and submm surveys are yet to be completed.

Band Depth Units	2–10 keV CGI	*u*, *g*, *r*, *i*, *z* mag	R mag	*H* mag	*K* mag	6.7 mJy	15 mJy	90 mJy	175 mJy	850 mJy	21 cm mJy
				N1							
Area	0.07	9	3.1	0.5	0.4		2.6	2.6	2	0.05	1.54
Depth	10^{-14}	23.3, 24.2, 23.5, 22.7, 21.1	23	19.5	18.0	1	3	100	100	8	0.1–0.4
N2											
Area	0.07	2	3.6	0.5	0.4	2.7	2.7	2.7	1	0.05	1.54
Depth	10^{-14}	22.5, 24.2, 23.5, 22.7, 21.1	23	19.5	18.0	1	3	100	100	8	0.1–0.4
N3											
Area		1, 1, 2.3, 1, 0	2.3	1		1.32	0.9	1.76			1.14
Depth		22.5, 23, 23, 23, 0	23	19.5		1	3	100			0.1–0.4
S1											
Area	2	1.2, 0, 4, 3, 0	4			1.8	4	4			4
Depth	10^{-13}	23, 0, 23.5, 23, 0	23.5			1	3	100			0.24

Until now the ELAIS northern fields have been only moderately surveyed spectroscopically. We have used the Calar Alto 2.2-m telescope and the Calar Alto Faint Object Spectrograph (CAFOS) for sources brighter than 17 (Gonzalez-Solares et al., in preparation) and the Calar Alto 3.5-m telescope and the Multi Object Spectrograph (MOSCA) for the fainter sources (Surace et al., in preparation). 29 ELAIS objects have been observed during the period 1998 May–July (of which 14 had $m > 19$). These observations have been completed with 29 field galaxies chosen in the same region for comparison purpose. From these northern samples most sources show strong starburst signatures up to $z = 0.5$ although two AGNs and one $z = 1.2$ quasar stellar object have been detected, these samples will be discussed in a forthcoming paper.

A number of programmes have been instigated to obtain more specific photometric and spectroscopic data of the infrared selected sources over a wider wavelength range. Some examples are detailed below:

(i) We have observed (Héraudeau et al., in preparation) about 150 sources in pointing observations in the S1 field using IRAC2 on the ESO/MPG 2.2-m telescope 1997 October, 1998 June and SOFI on the NTT 1998 October

(ii) Near-infrared H+K band spectroscopy of a small subset of sources with SOFI on the NTT (Alexander et al., in preparation).

8 CONCLUSIONS

In this paper we have described the motivation behind ELAIS, the largest non-serendipitous survey performed by *ISO*. Our primary goals in conducting the survey were to determine the relative importance and recent evolution of the dust-obscured mode of star formation in galaxies, and to constrain AGN unification models, and we detailed above how these influenced our selection of survey fields and observational parameters. The fields that have been covered by *ISO* are also being extensively mapped from radio to X-ray wavelengths as part of a concerted ground-based follow-up programme, whose multi-wavelength coverage will make the ELAIS regions fertile ground for undertaking future astrophysical investigations extending well beyond our initial survey aims.

Subsequent papers in this series will discuss in detail the scientific results from the ELAIS 'preliminary analysis' and 'final analysis'. The first of these papers will include: discussions of the extragalactic counts from the 'preliminary analysis' at 7 and 15 μm (Serjeant et al. 2000), and at 90 μm (Efstathiou et al., 2000); discussion of the stellar calibration and counts (Crockett et al., in preparation); and a discussion of sources detected in the multiply-repeated areas (Oliver et al., in preparation). Preliminary ELAIS data products were released through our WWW page (`http://athena.ph.ic.ac.uk/`), which also contains further details on the programme and the follow-up campaign.

ACKNOWLEDGMENTS

This paper is based on observations with *ISO*, an ESA project, with instruments funded by ESA Member States (especially the PI countries: France, Germany, the Netherlands and the United Kingdom) and with participation of ISAS and NASA.

The ISOCAM data presented in this paper was analysed using 'CIA', a joint development by the ESA Astrophysics Division and the ISOCAM Consortium. The ISOCAM Consortium is led by the ISOCAM PI, C. Cesarsky, Direction des Sciences de la Matiere, C. E. A., France. PIA is a joint development by the ESA Astrophysics Division and the ISOPHOT Consortium. The ISOPHOT Consortium is led by the Max-Planck-Institut fuër Astronomie (MPIA), Heidelberg, Germany. Contributing ISOPHOT Consortium institutes to the PIA development are: DIAS (Dublin Institute for advanced studies, Ireland) MPIK (Max-Planck-Institut fuër Kernphysik, Heidelberg, Germany), RAL (Rutherford Appleton Laboratory, Chilton, UK), AIP (Astronomisches Institut Potsdam, Germany) and MPIA.

This work in part was supported by PPARC (grant number GR/K98728) and by the EC TMR Network programme (FMRX-CT96-0068).

We would like to thank all the *ISO* staff at Vilspa both on the science team and on the Instrument Development Teams for their eternal patience in dealing with the wide variety of problems that a large programme like this presented.

REFERENCES

Antonucci R., 1993, ARA&A, 31, 473

Antonucci R. R. J., Miller J. S., 1985, ApJ, 297, 621

Aussel H., Cesarsky C. J., Elbaz D., Starck J. L., 1999, A&A, 342, 313
Barger A. J., Cowie L. L., Sanders D. B., Fulton E., Taniguchi Y., Sato Y., Kawara K., Okuda H., 1998, Nat, 394, 248
Barthel P. D., 1989, ApJ, 336, 606
Blain A. W., Kneib J.-P., Ivison R. J., Smail I., 1999, ApJL, 512, L87
Bogun S. et al., 1996, A&A, 315, L71
Cesarsky C. J. et al., 1996, A&A, 315, L32
Ciliegi P. et al., 1999, MNRAS, 302, 222
Clements D. L., Sutherland W. J., Saunders W., Efstathiou G. P., McMahon R. G., Maddox S., Lawrence A., Rowan-Robinson M., 1996, MNRAS, 279, 459
Clements D. L., Desert F.-X., Franceschini A., Reach W. T., Baker A. C., Davies J. K., Cesarsky C., 1999, A&A, 346, 383
Comastri A., Setti G., Zamorani G., Hasinger G., 1995, A&A, 296, 1
Condon J. J., 1992, ARA&A, 30, 575
Condon J. J., Mitchell K. J., 1984, AJ, 89, 610
Dole H. et al., 1999, in Cox P., Kessler M. F., eds, The Universe as seen by ISO. ESA Special Publications Series, UNESCO, Paris, p. 1031
Douglas J. N., Bash F. N., Bozyan F. A., Torrence G. W., Wolfe C., 1996, AJ, 111
Eales S., Lilly S., Gear W., Dunne L., Bond J. R., Hammer F., Le Fèvre O., Crampton D., 1999, ApJ, 515, 518
Efstathiou G. et al., 2000, MNRAS, submitted
Elbaz D. et al., 1999, in Cox P., Kessler M. F., eds, The Universe as seen by ISO. ESA Special Publications Series, UNESCO, Paris, p. 999
Fabian A. C., Iwasawa K., 1999, MNRAS, 303, L34
Fixsen D. J., Dwek E., Mather J. C., Bennett C. L., Shafer R. A., 1998, ApJ, 508, 123
Flores H. et al., 1999a, ApJ, 517, 148
Flores H. et al., 1999b, A&A, 343, 389
Franceschini A., Mazzei P., De Zotti G., Danese L., 1994, ApJ, 427, 140
Gabriel C., Acosta-Pulido J., Heinrichsen I., Skaley D., Morris H., Tai W.-M., 1997, in Hunt G., Payne H. E., eds, Proc. of the ADASS VI Conference, ASP Conf. Ser. Vol. 125. Astron. Soc. Pac., San Francisco, p. 108
Galaz G., De Lapparent V., 1998, A&A, 332, 459
Genzel R. et al., 1998, ApJ, 498, 579
Gruppioni C., Mignoli M., Zamorani G., 1999a, MNRAS, 304, 199
Gruppioni C. et al., 1999b, MNRAS, 305, 297
Guiderdoni B., Hivon E., Bouchet F. R., Maffei B., 1998, MNRAS, 295, 877
Halpern J. P., Moran E. C., 1998, ApJ, 494, 194
Hauser M. G. et al., 1998, ApJ, 508, 25
Helou G., Soifer B. T., Rowan-Robinson M., 1985, ApJL, 298, L7
Hopkins A. M., Mobasher B., Cram L., Rowan-Robinson M., 1998, MNRAS, 296, 839
Hughes D. H. et al., 1998, Nat, 394, 241
Kawara K. et al., 1998, A&A, 336, L9
Kessler M. F. et al., 1996, A&A, 315, L27
Lagache G., Abergel A., Boulanger F., Puget J. L., 1998, A&A, 333, 709
Lawrence A., 1999, Adv. Space Res., 23, 1167
Lawrence A., Rowan-Robinson M., Leech K., Jones D. H. P., Wall J. V., 1989, MNRAS, 240, 329
Lawrence A. et al., 2000, MNRAS, 308, 897
Leech K. J., Rowan-Robinson M., Lawrence A., Hughes J. D., 1994, MNRAS, 267, 253
Lemke D. et al., 1996, A&A, 315, L64
Linden-Vørnle M. J. D., 1997, in Laureijs R., Levine D., eds, Taking *ISO* to the Limits. ESA Publications, Noordwijk
Lutz D., Spoon H. W. W., Rigopoulou D., Moorwood A. F. M., Genzel R., 1998, ApJL, 505, L103
Lutz D., Veilleux S., Genzel R., 1999, ApJL, 517, L13
McHardy I. M. et al., 1998, Astron. Nachr., 319, 51
Madau P., Ferguson H. C., Dickinson M. E., Giavalisco M., Steidel C. C., Fruchter A., 1996, MNRAS, 283, 1388
Oliver S. J., Rowan-Robinson M., Saunders W., 1992, MNRAS, 256, 15P
Oliver S. et al., 1995, in Maddox S. J., Aragon-Salamanca A., eds, Wide-Field Spectroscopy and the Distant Universe. World Scientific, Singapore, p. 264
Ott S. et al., 1998, The CIA Manual. CEA-Saclay, Gif sur Yvette
Peacock J. A., Dodds S. J., 1994, MNRAS, 267, 1020
Pearson C., Rowan-Robinson M., 1996, MNRAS, 283, 174
Puget J.-L., Abergel A., Bernard J.-P., Boulanger F., Burton W. B., Desert F.-X., Hartmann D., 1996, A&A, 308, L5
Rigopoulou D. et al., 1999, AJ, 118, 2625
Röettgering H. J. A., Van Ojik R., Miley G. K., Chambers K. C., Van Breugel W. J. M., De Koff S., 1997, A&A, 326, 505
Rowan-Robinson M., Efstathiou A., 1993, MNRAS, 263, 675
Rowan-Robinson M., Harris S., 1983, MNRAS, 202, 767
Rowan-Robinson M. et al., 1991a, Nat, 351, 719
Rowan-Robinson M., Jones M., Leech K., Vedi K., Hughes J., 1991b, MNRAS, 249, 729
Sanders D. B., Mirabel I. F., 1996, ARA&A, 34, 749
Sanders D. B., Soifer B. T., Elias J. H., Madore B. F., Matthews K., Neugebauer G., Scoville N. Z., 1988, ApJ, 325, 74
Sanders D. B., Surace J. A., Ishida C. M., 1999, in Barnes J. E., Sanders D. B., eds, IAU Symp. 186, Galaxy Interactions at Low and High Redshift, p. 289
Saunders W., Frenk C., Rowan-Robinson M., Lawrence A., Efstathiou G., 1991, Nat, 349, 32
Scheuer P. A. G., 1987, in Zenus J. A., Pearson T. J., eds, Superluminal Radio Sources, Vol. 194. Cambridge Univ. Press, Cambridge
Schlegel D. J., Finkbeiner D. P., Davis M., 1998, ApJ, 500, 525
Serjeant S. B. G. et al., 1997, MNRAS, 289, 457
Serjeant S. B. G. et al., 2000, MNRAS, 316, 768 (Paper II, this issue)
Siebenmorgen R. et al., 1996, A&A, 315, L169
Smail I., Ivison R. J., Blain A. W., 1997, ApJL, 490, L5
Steidel C. C., Adelberger K. L., Giavalisco M., Dickinson M., Pettini M., 1999, ApJ, 519, 1
Taniguchi Y. et al, 1997a, in Laureijs R., Levine D., eds, Taking *ISO* to the Limits. ESA Publications, Noordwijk
Taniguchi Y. et al., 1997b, A&A, 328, L9
van Ojik R., Rottgering H. J. A., Miley G. K., Bremer M. N., Macchetto F., Chambers K. C., 1994, A&A, 289, 54
Veilleux S., Kim D.-C., Sanders D. B., Mazzarella J. M., Soifer B. T., 1995, ApJS, 98, 171
Veilleux S., Kim D.-C., Sanders D. B., 1999, ApJ, 522, 113
Windhorst R. A., 1984, PhD thesis, Univ. Leiden
Windhorst R. A., Miley G. K., Owen F. N., Kron R. G., Koo D. C., 1985, ApJ, 289, 494
Windhorst R. A. et al., 1991, ApJ, 380, 362
Windhorst R. A., Keel W. C., Pascarelle S. M., 1998, ApJL, 494, L27

APPENDIX A: LOG OF THE *ISO* OBSERVATIONS

In Table A1 we present a list of all the observations performed by *ISO* as part of the ELAIS raster observations. We do not include the observations performed as part of the *ISO* photometric follow-up of ELAIS sources which are available on our WWW pages `http://athena.ph.ic.ac.uk/`. Table A2 details those observations which have had some instrument or telemetry problems as flagged at Vilspa or for which we have noted peculiarities.

Table A1. Log of all the ISO survey observations performed for ELAIS, excluding the pointed photometric observations. TDN is a unique identifier for each *ISO* observation and monotonically increased throughout the mission. OFFICIAL_NAME is a unique identifier for ELAIS observations constructed from the instrument name, the filter, the main field identifier and where required a subfield identifier and a multiplicity identifier, it does not correspond to the name in the *ISO* archives.

TDN	OFFICIAL_NAME	RA (J2000) Dec(J2000)	ROLL	M	N	DM	DN	TINT	FILT	STATUS
11600721	CAM_LW3_N2_T_I	16 35 45.00 +41 06 00.0	84	28	14	90	180	21	LW3	Observed
19201010	PHT_C90_N1_T_I	16 10 01.20 +54 30 36.0	358	10	20	130	130	10	90	Observed
19201091	PHT_C90_N1_T_J	16 10 01.20 +54 30 36.0	358	10	20	130	130	32	90	Observed
23200251	CAM_LW3_S1_1	00 30 25.40 −42 57 00.3	77	28	14	90	180	21	LW3	Observed
23200252	PHT_C90_S1_1A	00 30 14.90 −42 47 11.7	78	10	20	130	130	20	90	Observed
23200289	PHT_C90_S1_1B	00 30 36.00 −43 06 48.8	78	10	20	130	130	20	90	Observed
23200353	CAM_LW3_S1_2	00 31 08.20 −43 36 14.1	78	28	14	90	180	21	LW3	Observed
23200354	PHT_C90_S1_2A	00 30 57.40 −43 26 25.7	78	10	20	130	130	20	90	Observed
23200392	PHT_C90_S1_2B	00 31 19.00 −43 46 02.5	78	10	20	130	130	20	90	Observed
23300257	CAM_LW3_S1_4	00 33 59.40 −42 49 03.1	77	28	14	90	180	21	LW3	Observed
23300258	PHT_C90_S1_4A	00 33 48.30 −42 39 15.8	77	10	20	130	130	20	90	Observed
23300294	PHT_C90_S1_4B	00 34 10.60 −42 58 50.4	78	10	20	130	130	20	90	Observed
23300459	CAM_LW3_S1_5	00 34 44.40 −43 28 12.0	78	28	14	90	180	21	LW3	Observed
23300460	PHT_C90_S1_5A	00 34 33.10 −43 18 24.9	78	10	20	130	130	20	90	Observed
23300495	PHT_C90_S1_5B	00 34 55.80 −43 37 59.1	78	10	20	130	130	20	90	Observed
30200101	CAM_LW3_N1_1	16 15 01.00 +54 20 41.0	258	28	14	90	180	21	LW3	Observed
30200102	PHT_C90_N1_1A	16 15 16.70 +54 10 57.0	258	10	20	130	130	20	90	Observed
30200113	PHT_C90_N1_1B	16 14 45.30 +54 30 24.9	258	10	20	130	130	20	90	Observed
30400103	CAM_LW3_N1_2	16 13 57.10 +54 59 35.9	255	28	14	90	180	21	LW3	Aborted
30400104	PHT_C90_N1_2A	16 14 13.30 +54 49 52.4	256	10	20	130	130	20	90	Failed
30400114	PHT_C90_N1_2B	16 13 40.90 +55 09 19.3	255	10	20	130	130	20	90	Aborted
30500105	CAM_LW3_N1_3	16 10 34.90 +54 11 12.7	254	28	14	90	180	21	LW3	Observed
30500106	PHT_C90_N1_3A	16 10 51.50 +54 01 30.9	254	10	20	130	130	20	90	Observed
30500115	PHT_C90_N1_3B	16 10 18.10 +54 20 54.4	254	10	20	130	130	20	90	Observed
30600107	CAM_LW3_N1_4	16 09 27.00 +54 49 58.7	253	28	14	90	180	21	LW3	Observed
30600108	PHT_C90_N1_4A	16 09 44.20 +54 40 17.4	253	10	20	130	130	20	90	Observed
30600116	PHT_C90_N1_4B	16 09 09.70 +54 59 39.8	252	10	20	130	130	20	90	Observed
30900111	CAM_LW3_N1_6	16 04 59.00 +54 39 44.3	249	28	14	90	180	21	LW3	Observed
30900112	PHT_C90_N1_6A	16 05 17.20 +54 30 05.5	249	10	20	130	130	20	90	Observed
30900118	PHT_C90_N1_6B	16 04 40.70 +54 49 22.9	249	10	20	130	130	20	90	Observed
31000109	CAM_LW3_N1_5	16 06 10.80 +54 01 08.0	248	28	14	90	180	21	LW3	Observed
31000117	PHT_C90_N1_5B	16 05 53.10 +54 10 47.3	248	10	20	130	130	20	90	Observed
31000132	PHT_C90_N1_5A	16 06 28.40 +53 51 28.6	248	10	20	130	130	20	90	Observed
40700479	CAM_LW3_X6_1	14 36 43.10 +15 44 13.0	124	12	6	90	180	21	LW3	Observed
40700480	PHT_C90_X6_1	14 36 43.10 +15 44 13.0	124	9	9	130	130	20	90	Observed
40701983	CAM_LW3_X4_1	17 14 14.00 +50 15 23.6	163	12	6	90	180	21	LW3	Observed
40701984	PHT_C90_X4_1	17 14 14.00 +50 15 23.6	162	9	9	130	130	20	90	Observed
40800464	PHT_C90_S1_7A	00 37 20.80 −42 30 55.3	251	10	20	130	130	20	90	Observed
40800497	PHT_C90_S1_7B	00 37 44.20 −42 50 27.1	251	10	20	130	130	20	90	Observed
40800663	CAM_LW3_S1_7	00 37 32.50 −42 40 41.2	251	28	14	90	180	21	LW3	Observed
40800765	CAM_LW3_S1_8	00 38 19.60 −43 19 44.5	251	28	14	90	180	21	LW3	Observed
41000856	PHT_C90_S1_3A	00 31 40.90 −44 05 38.9	254	10	20	130	130	20	90	Observed
41000893	PHT_C90_S1_3B	00 32 03.00 −44 25 15.0	254	10	20	130	130	20	90	Observed
41001062	PHT_C90_S1_6A	00 35 18.80 −43 57 33.0	253	10	20	130	130	20	90	Observed
41001096	PHT_C90_S1_6B	00 35 42.00 −44 17 06.4	253	10	20	130	130	20	90	Observed
41001161	CAM_LW3_S1_6	00 35 30.40 −44 07 19.8	253	28	14	90	180	21	LW3	Observed
41101867	CAM_LW3_S1_9	00 39 07.80 −43 58 46.6	253	28	14	90	180	21	LW3	Observed
41300766	PHT_C90_S1_8A	00 38 07.70 −43 09 58.8	255	10	20	130	130	20	90	Failed
41300798	PHT_C90_S1_8B	00 38 31.60 −43 29 30.2	255	10	20	130	130	32	90	Aborted
41300955	CAM_LW3_S1_3	00 31 51.90 −44 15 27.0	256	28	14	90	180	21	LW3	Observed
41301068	PHT_C90_S1_9A	00 38 55.70 −43 49 01.2	255	10	20	130	130	20	90	Observed
41301099	PHT_C90_S1_9B	00 39 20.00 −44 08 31.8	255	10	20	130	130	20	90	Observed
41502787	CAM_LW3_X3_1	00 22 48.00 −30 06 30.0	254	16	16	90	90	21	LW3	Observed
41502788	PHT_C90_X3_1	00 22 48.00 −30 06 30.0	254	12	12	130	130	20	90	Observed
42500136	PHT_C90_N3_2A	14 25 49.90 +33 09 53.8	114	10	20	130	130	20	90	Observed
42500146	PHT_C90_N3_2B	14 25 18.60 +32 51 00.7	114	10	20	130	130	20	90	Observed
42500237	CAM_LW3_N3_3	14 29 38.30 +33 24 49.6	114	28	14	90	180	21	LW3	Observed
42700238	PHT_C90_N3_3A	14 29 54.50 +33 34 14.2	113	10	20	130	130	20	90	Observed
42700247	PHT_C90_N3_3B	14 29 22.10 +33 15 24.9	113	10	20	130	130	20	90	Observed
43800341	CAM_LW3_N3_5	14 32 38.20 +33 11 10.3	105	28	14	90	180	21	LW3	Observed
49900120	PHT_C90_N2_1A	16 32 33.00 +41 22 14.3	247	20	20	75	130	12	90	Observed
49900222	PHT_C90_N2_1B	16 33 26.50 +41 04 51.7	247	20	20	75	130	12	90	Observed
49900326	PHT_C90_N2_2B	16 35 10.50 +40 30 02.0	248	20	20	75	130	12	90	Observed
50000124	PHT_C90_N2_2A	16 34 18.30 +40 47 27.6	247	20	20	75	130	12	90	Observed
50000228	PHT_C90_N2_3A	16 35 39.40 +41 41 55.6	247	20	20	75	130	12	90	Observed
50000330	PHT_C90_N2_3B	16 36 31.30 +41 24 27.7	247	20	20	75	130	12	90	Observed
50000723	CAM_LW3_N2_3	16 36 05.50 +41 33 11.8	247	28	14	90	180	21	LW3	Observed
50100172	PHT_C90_N2_4B	16 38 14.20 +40 49 27.6	246	20	20	75	130	12	90	Observed

Table A1 – *continued*

TDN	OFFICIAL_NAME	RA (J2000) Dec(J2000)	ROLL	M	N	DM	DN	TINT	FILT	STATUS
50100273	PHT_C90_N2_5A	16 38 47.80 +42 01 18.0	246	20	20	75	130	12	90	Observed
50100374	PHT_C90_N2_5B	16 39 39.70 +41 43 44.9	246	20	20	75	130	12	90	Observed
50100727	CAM_LW3_N2_5	16 39 13.80 +41 52 31.6	246	28	14	90	180	21	LW3	Observed
50100871	PHT_C90_N2_4A	16 37 23.50 +41 06 58.3	246	20	20	75	130	12	90	Observed
50200119	CAM_LW3_N2_1	16 32 59.80 +41 13 33.2	244	28	14	90	180	21	LW3	Observed
50200225	CAM_LW3_N2_4	16 37 48.90 +40 58 13.1	245	28	14	90	180	21	LW3	Observed
50200429	CAM_LW3_N2_6	16 40 55.50 +41 17 22.7	246	28	14	90	180	21	LW3	Observed
50200575	PHT_C90_N2_6A	16 40 30.10 +41 26 10.4	246	20	20	75	130	12	90	Observed
51100131	CAM_LW3_N2_2	16 34 44.50 +40 38 45.0	236	28	14	90	180	21	LW3	Observed
51100234	CAM_LW2_N2_4	16 37 48.90 +40 58 13.1	236	28	14	90	180	21	LW2	Observed
51100736	CAM_LW2_N2_6	16 40 55.50 +41 17 22.7	237	28	14	90	180	21	LW2	Observed
51100835	CAM_LW2_N2_5	16 39 13.80 +41 52 31.6	236	28	14	90	180	21	LW2	Observed
51200131	CAM_LW2_N2_1	16 32 59.80 +41 13 33.2	234	28	14	90	180	21	LW2	Observed
51200232	CAM_LW2_N2_2	16 34 44.50 +40 38 45.0	235	28	14	90	180	21	LW2	Observed
51200433	CAM_LW2_N2_3	16 36 05.50 +41 33 11.8	235	28	14	90	180	21	LW2	Observed
51200576	PHT_C90_N2_6B	16 41 20.80 +41 08 34.6	236	20	20	75	130	12	90	Observed
54502485	CAM_LW3_X1_1	01 13 12.80 −45 14 06.7	33	16	8	90	180	21	LW3	Observed
54502486	PHT_C90_X1_1	01 13 12.80 −45 14 06.7	33	12	12	130	130	20	90	Observed
59800143	CAM_LW2_S1_5	00 34 44.40 −43 28 12.0	76	28	14	90	180	21	LW2	Observed
59800244	CAM_LW2_S1_6	00 35 30.40 −44 07 19.8	77	28	14	90	180	21	LW2	Observed
59800745	CAM_LW2_S1_8	00 38 19.60 −43 19 44.5	77	28	14	90	180	21	LW2	Observed
59800846	CAM_LW2_S1_9	00 39 07.80 −43 58 46.6	77	28	14	90	180	21	LW2	Observed
61300341	CAM_LW2_N3_5	14 32 38.20 +33 11 10.3	291	28	14	90	180	21	LW2	Observed
61600642	PHT_C90_N3_5A	14 32 54.70 +33 20 33.4	289	20	20	75	130	12	90	Observed
61600649	PHT_C90_N3_5B	14 32 21.70 +33 01 47.0	289	20	20	75	130	12	90	Observed
61800277	CAM_LW3_X2_1	13 34 36.00 +37 54 36.0	280	16	8	90	180	21	LW3	Observed
61800278	PHT_C90_X2_1	13 34 36.00 +37 54 36.0	279	12	12	130	130	20	90	Observed
62300324	CAM_LW2_N3_6D	14 32 01.00 +32 20 47.0	285	14	7	90	180	21	LW2	Observed
62300422	CAM_LW2_N3_6B	14 30 32.00 +32 27 37.0	284	14	7	90	180	21	LW2	Observed
63500448	PHT_C90_N3_6D	14 32 01.00 +32 20 47.0	277	10	20	130	65	12	90	Observed
63500539	PHT_C90_N3_4C	14 29 34.80 +32 53 13.0	276	10	20	130	65	12	90	Observed
63500628	PHT_C90_N3_1D	14 27 06.80 +33 25 28.0	275	10	20	130	65	12	90	Observed
63500726	PHT_C90_N3_1B	14 25 36.30 +33 32 04.0	275	10	20	130	65	12	90	Observed
63500825	PHT_C90_N3_1A	14 26 07.90 +33 50 57.0	275	10	20	130	65	12	90	Observed
63501041	PHT_C90_N3_5C_I	14 32 09.70 +33 24 00.0	276	10	20	130	65	12	90	Observed
63501142	PHT_C90_N3_5D_I	14 31 36.90 +33 05 13.0	276	10	20	130	65	12	90	Observed
63800106	CAM_LW2_N3_2B	14 24 33.60 +32 54 17.0	273	14	7	90	180	21	LW2	Observed
63800205	CAM_LW2_N3_2A	14 25 04.80 +33 13 11.0	273	14	7	90	180	21	LW2	Observed
63800302	CAM_LW2_N3_1B	14 25 36.30 +33 32 04.0	273	14	7	90	180	21	LW2	Observed
63800401	CAM_LW2_N3_1A	14 26 07.90 +33 50 57.0	273	14	7	90	180	21	LW2	Observed
63800504	CAM_LW2_N3_1D	14 27 06.80 +33 25 28.0	272	14	7	90	180	21	LW2	Observed
63800603	CAM_LW2_N3_1C	14 27 38.70 +33 44 19.0	272	14	7	90	180	21	LW2	Observed
63800745	PHT_C90_N3_6A	14 31 04.40 +32 46 25.0	273	10	20	130	65	12	90	Failed
67200103	CAM_LW3_N1_2_I	16 13 57.10 +54 59 35.9	254	28	14	90	180	21	LW3	Observed
67200114	PHT_C90_N1_2C	16 12 49.40 +54 57 15.1	254	20	20	130	65	20	90	Observed
67500104	PHT_C90_N1_1C_I	16 13 54.30 +54 18 22.3	251	20	20	130	65	12	90	Observed
75200310	PHT_C90_N1_T_K	16 11 09.60 +54 31 52.7	171	10	20	130	130	12	90	Observed
75200411	PHT_C90_N1_T_L	16 08 52.90 +54 29 16.9	170	10	20	130	130	12	90	Observed
75200512	PHT_C90_N1_T_M	16 09 52.10 +54 40 30.9	170	20	10	130	130	12	90	Observed
75200613	PHT_C90_N1_T_F	16 10 10.10 +54 20 41.1	171	20	10	130	130	12	90	Observed
75901219	PHT_C90_S1_5_L	00 34 44.40 −43 28 12.0	242	14	14	130	130	12	90	Observed
76500218	PHT_C90_S1_5_K	00 34 44.40 −43 28 12.0	245	14	14	130	130	12	90	Observed
77001315	PHT_C90_N2_T_L	16 34 58.80 +41 01 05.1	157	10	20	130	130	12	90	Observed
77100214	PHT_C90_N2_T_K	16 36 31.30 +41 10 53.8	156	10	20	130	130	12	90	Observed
77400316	PHT_C90_N2_T_M	16 35 18.90 +41 14 42.7	153	20	10	130	130	12	90	Observed
77400417	PHT_C90_N2_T_F	16 36 11.00 +40 57 17.0	153	20	10	130	130	12	90	Observed
77500166	PHT_C90_S1_8A	00 38 07.70 −43 09 58.8	252	20	20	65	130	12	90	Observed
77500207	CAM_LW3_S1_5_K	00 34 44.40 −43 28 12.0	252	28	14	90	180	21	LW3	Observed
77800367	CAM_LW3_N1_U_J	16 11 00.40 +54 13 25.4	145	8	4	90	180	21	LW3	Observed
77800368	CAM_LW3_N1_U_K	16 11 00.40 +54 13 25.4	145	8	4	90	180	21	LW3	Observed
77800369	CAM_LW3_N1_U_L	16 11 00.50 +54 13 31.3	145	8	4	90	180	21	LW3	Observed
77800370	CAM_LW3_N1_U_M	16 11 00.50 +54 13 31.3	145	8	4	90	180	21	LW3	Observed
77800371	CAM_LW3_N1_U_N	16 11 00.90 +54 13 21.7	145	8	4	90	180	21	LW3	Observed
77800372	CAM_LW3_N1_U_O	16 11 00.90 +54 13 21.7	145	8	4	90	180	21	LW3	Observed
77900101	CAM_LW3_N2_T_J	16 35 45.00 +41 06 00.0	148	28	14	90	180	21	LW3	Observed
77900202	CAM_LW2_N2_T_J	16 35 45.00 +41 06 00.0	148	28	14	90	180	21	LW2	Observed
78500120	PHT_C160_N2_U_I	16 35 50.00 +41 32 33.1	142	13	13	96	96	16	160	Observed
78500221	PHT_C160_N2_U_J	16 35 44.10 +41 31 29.0	142	13	13	96	96	16	160	Observed
78500322	PHT_C160_N2_V_I	16 34 39.70 +41 19 42.7	141	13	13	96	96	16	160	Observed
78502406	CAM_LW3_S1_5_J	00 34 44.40 −43 28 12.0	261	28	14	90	180	21	LW3	Observed
78600108	CAM_LW2_S1_5_J	00 34 44.40 −43 28 12.0	261	28	14	90	180	21	LW2	Observed

Table A1 – *continued*

TDN	OFFICIAL_NAME	RA (J2000) Dec(J2000)	ROLL	M	N	DM	DN	TINT	FILT	STATUS
78700123	PHT_C160_N2_V_J	16 34 33.80 +41 18 38.6	139	13	13	96	96	16	160	Observed
78700224	PHT_C160_N2_W_I	16 33 29.80 +41 06 49.7	139	13	13	96	96	16	160	Observed
78700325	PHT_C160_N2_W_J	16 33 24.00 +41 05 45.6	139	13	13	96	96	16	160	Observed
78800126	PHT_C160_N2_X_I	16 36 58.20 +41 19 19.9	139	13	13	96	96	16	160	Observed
78800227	PHT_C160_N2_X_J	16 36 52.40 +41 18 15.8	139	13	13	96	96	16	160	Observed
78800328	PHT_C160_N2_Y_I	16 35 47.90 +41 06 32.0	139	13	13	96	96	16	160	Observed
79400232	PHT_C160_N2_E_I	16 38 06.00 +41 06 04.1	133	13	13	96	96	16	160	Observed
79400333	PHT_C160_N2_E_J	16 38 00.20 +41 05 00.0	133	13	13	96	96	16	160	Observed
79400434	PHT_C160_N2_F_I	16 36 55.70 +40 53 18.9	133	13	13	96	96	16	160	Observed
79500329	PHT_C160_N2_Y_J	16 35 42.10 +41 05 27.9	132	13	13	96	96	16	160	Observed
79500430	PHT_C160_N2_Z_I	16 34 38.10 +40 53 41.6	132	13	13	96	96	16	160	Observed
79500531	PHT_C160_N2_Z_J	16 34 32.30 +40 52 37.5	132	13	13	96	96	16	160	Observed
79600173	CAM_LW3_N1_U_P	16 11 00.40 +54 13 25.4	127	8	4	90	180	21	LW3	Observed
79600174	CAM_LW3_N1_U_Q	16 11 00.40 +54 13 25.4	127	8	4	90	180	21	LW3	Observed
79600175	CAM_LW3_N1_U_R	16 10 59.70 +54 13 23.1	127	8	4	90	180	21	LW3	Observed
79600176	CAM_LW3_N1_U_I	16 10 59.70 +54 13 23.1	127	8	4	90	180	21	LW3	Observed
79800135	PHT_C160_N2_F_J	16 36 49.90 +40 52 14.8	129	13	13	96	96	16	160	Observed
79800236	PHT_C160_N2_G_I	16 35 45.90 +40 40 30.9	129	13	13	96	96	16	160	Observed
79800337	PHT_C160_N2_G_J	16 35 40.10 +40 39 26.9	129	13	13	96	96	16	160	Observed
80600181	CAM_LW3_X5_1	02 14 17.20 −11 58 46.2	254	12	12	90	90	21	LW3	Observed
86800640	PHT_C90_S2_1_J	05 02 25.70 −30 36 24.0	287	18	9	65	130	12	90	Observed
86901244	PHT_C90_S2_1_L	05 02 22.10 −30 36 21.9	288	9	9	130	130	20	90	Observed
86901341	CAM_LW3_S2_1_J	05 02 24.30 −30 36 04.7	288	14	7	90	180	21	LW3	Observed
86901445	CAM_LW3_S2_1_L	05 02 23.60 −30 36 04.3	288	14	7	90	180	21	LW3	Observed
86901539	CAM_LW3_S2_1_I	05 02 24.00 −30 36 00.0	288	14	7	90	180	21	LW3	Observed
87001338	PHT_C90_S2_1_I	05 02 24.00 −30 36 00.0	289	9	18	130	65	12	90	Observed
87001442	PHT_C90_S2_1_K	05 02 25.90 −30 35 38.1	289	18	9	65	130	12	90	Observed
87001743	CAM_LW3_S2_1_K	05 02 24.40 −30 35 55.7	289	14	7	90	180	21	LW3	Observed
87001846	PHT_C90_S2_1_M	05 02 22.30 −30 35 36.0	289	9	9	130	130	20	90	Observed
87001909	PHT_C160_S2_1_M	05 02 22.30 −30 35 36.0	289	12	12	96	96	32	160	Observed
87500403	PHT_C160_S2_1_K	05 02 25.90 −30 35 38.1	293	6	12	180	96	32	160	Observed
87500705	PHT_C160_S2_1_L	05 02 22.10 −30 36 21.9	293	6	12	180	96	32	160	Observed
87500808	CAM_LW2_S2_1_M	05 02 23.70 −30 35 55.3	293	14	7	90	180	21	LW2	Observed

Table A2. List of observations with telemetry or similar instrument problems.

TDN	Name	Description
19201091	PHT_C90_N1_T_J	Very high glitch rate owing to position in orbit
23300257	CAM_LW3_S1_4	Telemetry drops caused some science data to be lost
30400104	PHT_C90_N1_2A	failed owing to telemetry drops
41001062	PHT_C90_S1_6A	Vilspa flagged as ‘Unknown quality’
41001161	CAM_LW3_S1_6	Vilspa flagged as ‘Unknown quality’
41300766	PHT_C90_S1_8A	failed owing to telemetry drops
63800745	PHT_C90_N3_6A	failed owing to instrument problems
77400417	PHT_C90_N2_T_F	Vilspa flagged as ‘Unknown quality’
87500403	PHT_C160_S2_1_K	Instrument problems (warm up)
87500705	PHT_C160_S2_1_L	Instrument problems (warm up)

This paper has been typeset from a TEX/LATEX file prepared by the author.